Final Draft
of the original manuscript:

Hegadekatte, V.; Hilgert, J.; Kraft, O.; Huber, N.:
Multi time scale simulations for wear prediction in micro-gears
In: Wear (2009) Elsevier

DOI: 10.1016/j.wear.2009.08.017

Multi time scale simulations for wear prediction in micro-gears

V. HEGADEKATTE[1, 2,*], J. HILGERT[2], O. KRAFT[1, 3], N. HUBER[2, 4,*]

[1]Institut für Zuverlässigkeit von Bauteilen und Systemen, Universität Karlsruhe (TH), Kaiserstrasse 12, D-76131, Karlsruhe, Germany.

[2]Institut für Werkstoffphysik und Technologie, Technische Universität Hamburg-Harburg, Eissendorfer Strasse 42(M), D-21073, Hamburg, Germany.

[3]Institut für Materialforschung II, Forschungszentrum Karlsruhe GmbH, Hermann von Helmholtz Platz 1, D-76344, Eggenstein-Leopoldshafen, Germany.

[4]Institut für Werkstoffforschung, GKSS-Forschungszentrum Geesthacht GmbH, Max-Planck-Strasse, D-21502, Geesthacht, Germany.

Abstract

Reliability of micro-gears is known to be adversely affected by wear. In this work we report a strategy to predict local wear with the aim of predicting their effective life span. For the prediction of local wear we start from the relevant model experiments, choice of a suitable wear model and identification of the wear coefficient from these experiments. This wear model is then implemented in an efficient finite element based scheme to predict local wear. Here we report the further development of this finite element based wear simulation tool, the Wear-Processor, to handle this multi time scale problem of gear tooth wear. It is needed to bridge the various time scales between the very fast pass of a contact over a surface point and the long-term wear simulation that is required for a prediction of the life span. Additionally it is necessary to account for any change in the slip rate due to wear. The results presented in this article show how fast the gear tooth geometry, the slip rates and the line of action deviate from their original values as a consequence of wear. We predict a maximum of 3 μm of wear on silicon nitride micro gear tooth flank with width of 200 μm just after 3500 contact cycles.

1 Introduction

Microsystems and micro-machines in particular are a rapidly emerging technology, finding a wide variety of applications. Tribology is expected to play a strong role in enabling microsystems technology because surface forces dominate body forces [1]. Wear being a surface phenomenon was identified as a critical factor for limiting their lifespan since Gabriel et al. [2] observed wear in a silicon surface micro-machined gear spun on its hub at high speed using an air jet. Williams [3] has shown that one minute of life for a micro-machine represents a degree of wear and degradation equal to more than

*Corresponding Authors:
- Novelis Technology (India), Taloja R & D Center, Hindalco Industries Ltd., Plot No. 2 MIDC Taloja, Navi Mumbai – 410208, India. E-mail: vishwanath.hegadekatte@adityabirla.com.
- norbert.huber@gkss.de (N. Huber)

ten years for a well designed watch bearing. Additionally, micro-machines like the ceramic micro planetary gear train shown in Figure 1 have fabrication tolerances that cannot be as stringent as in the macro world and there is hardly any possibility for correction to the specified tolerances after fabrication. However, Hall et al. [4] have suggested based on their experimental study that by patterning the side walls of the mold, the side walls of LIGA[1] parts can be engineered thus giving control over friction, adhesion and wear in LIGA devices. For the particular case of the planetary gear train, the number of teeth in the gear train has to be adjusted to be an integer and so it has a non

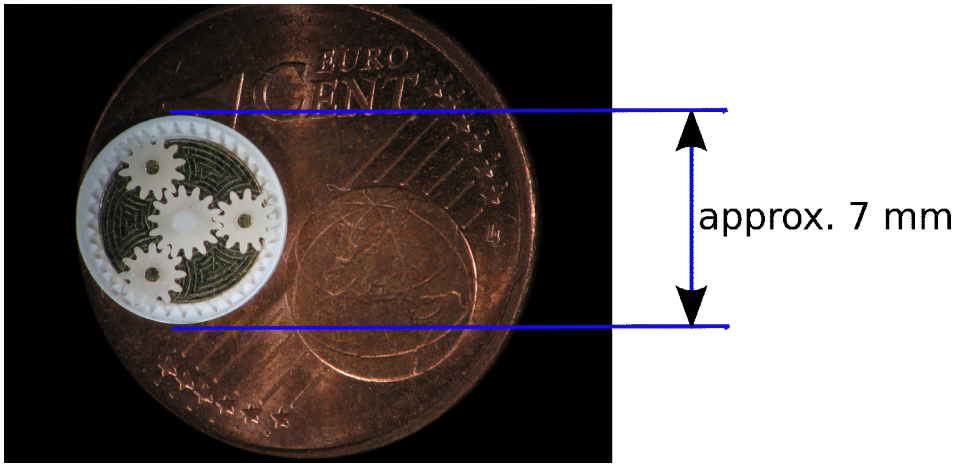

Figure 1: Micro planetary gear train made from ceramics pictured here on a one euro cent coin. It was fabricated at the Karlsruhe Institute of Technology within the collaborative research centre, SFB 499

ideal geometry to begin with, thus making it tribologically disadvantaged. Wear in engineering systems normally does not change the geometry in a way, that it has an effect on the kinematics of the system. Micro-machine designers have to take into account the fact that surfaces can wear considerably in relation to the dimension of the component and that the geometries change. Design for tribological performance should not always be based on the assumption that Hertzian loading conditions will be maintained, however in some cases assuming Hertzian loading may be a good approximation. New fabrication methods (see the volumes edited by Loehe & Hausselt [5]) for micro components have been developed by employing various wear resistant materials like ceramics. Such technologies have increased the choice of the available materials, thus giving larger room for micro-machine designers. However, the ability to predict wear and life-span is still essential for the development of reliable micro-machines.

Study of wear in micro-machines is often carried out using experimental techniques like pin-on-disc, twin-disc, scratch test, AFM etc. to characterize the tribological properties of various materials used for fabricating micro-machines. These experiments attempt to

[1] LIGA is a process developed at Forschungszentrum Karlsruhe that enables mass production of polymer micro components and it stands for the German acronym for Lithography, Electroforming and Plastics Molding

mimic the contact conditions of the micro-machine under study in terms of contact pressure, sliding velocity etc. The specimens in the tribometer have the same microstructure as the micro-machine itself and the loading chosen in the experiments are such that they mimic the actual condition (chapter 21 of [5]). For example, twin-disc rolling/sliding tribometer tries to mimic the rolling/sliding contact experienced by the teeth of two mating gears. Hegadekatte et al. [6, 7] proposed an approach that involves a computationally efficient incremental implementation of Archard's wear model [8] on the global scale for modeling sliding and rolling/sliding wear in such experiments. It was shown that this fast simplistic numerical tool can be used to identify the wear coefficient from pin-on-disc and twin-disc experimental data and also predict the wear depths within a limited range of parameter variation. It was also shown that the wear coefficient in the Archard's wear model identified on the global scale was also valid on the local scale. Tribometry allows for a qualitative study of the suitability of a particular material combination and therefore modeling of wear with data from such experiments is necessary in order to predict local wear in complex micro-machines with time dependent local pressure and slip. In this article we use the identified wear coefficient from model experiments to simulate local wear on a ceramic micro-gear tooth flank in a micro-planetary gear train shown in Figure 1.

For simulating wear in micro-machines, the Archard's wear model is the most popular model as discussed by Williams [3], where it is used to predict wear in rotating pivots for moving micro mechanical assemblies. Zhao & Chang [9] have developed a micro-contact and wear model for predicting the material removal rate from silicon wafer surfaces during chemical-mechanical polishing, where the developed equation is a representation of the Archard's wear law. Sawyer [10] used a simulation scheme based on the Archard's wear model for the surface shape and contact pressure evolution during copper chemical-mechanical polishing. Wu & Cheng [11, 12] proposed an analytical expression for partial elasto hydrodynamic lubricated contacts in spur gears and showed that the highest wear occurs at the beginning of engagement of the gears in the macro world. The micro planetary gear train shown in Figure 1 is expected to run also without lubrication and therefore we concentrate on unlubricated contacts in the present work. Simulation of unlubricated wear employing Archard's wear model for spur gears [13], helical gears [14] and conical gears [15] have been proposed by Andersson and co-workers.

In this work we report a strategy to predict local wear with the aim of predicting their effective life span. For the prediction of local wear we start from the relevant model experiments, choice of a suitable wear model and identification of the wear coefficient from these experiments. This wear model is then implemented in an efficient finite element based scheme to predict local wear. Here we report the further development of this finite element based wear simulation tool, the Wear-Processor [16], to handle the complex geometry of mating gear tooth and the multi time scale problem of gear tooth flank wear. This is needed to bridge the time scales between the very fast pass of a contact over a surface point and the long-term wear simulation that is required for a prediction of the life span. Additionally it is necessary to account for the change of pressure and the slip rate due to wear. Since the finite element method is used to solve the

contact problem explicitly, we do not invoke any simplifying assumption regarding the evolving geometry due to wear.

2 Experiments and wear coefficient identification

A selection of promising materials for fabricating the micro planetary gear train have been carried out using micro pin-on-disc and twin-disc tribometer (Figure 2 (a)). The

(a) (b)

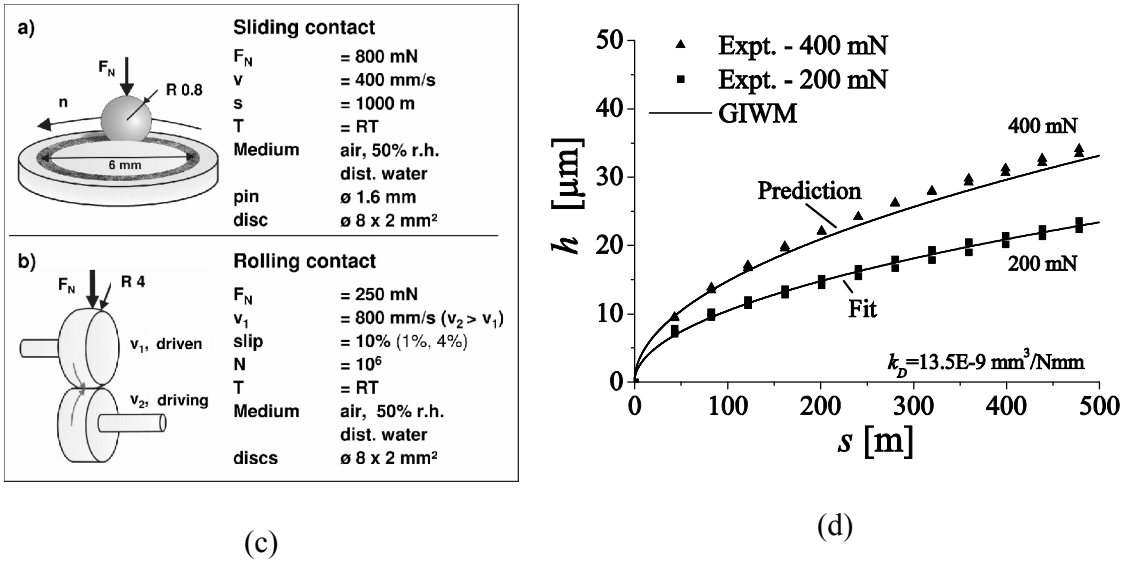

(c) (d)

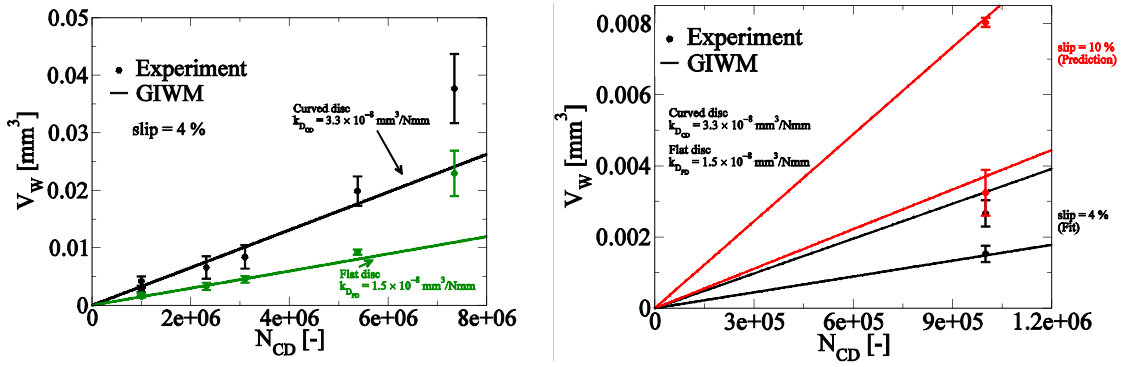

Figure 2: (a) Tribometry experimental setup for pin-on-disc and twin disc along with the various parameters. (b) Wear depth as a function of the sliding distance from pin-on-disc tribometer in comparison with results from GIWM. Volume of material removed from the GIWM in comparison with the experimental results from the twin-disc tribometer for the fit (c) at 4% slip and the prediction (d) for 10% slip

unidirectional sliding wear tests are mainly relevant for the gear axles, hub and the side surface of the gears in the gear train (Figure 1). The twin-disc experiments at different load and slip conditions are relevant to investigate the mixed type of rolling/ sliding wear, which is present in the gear tooth flank. Different candidate materials, such as silicon nitride and tungsten carbide among others have been rigorously tested using the setup by Kurzenhaeuser et al. [17].

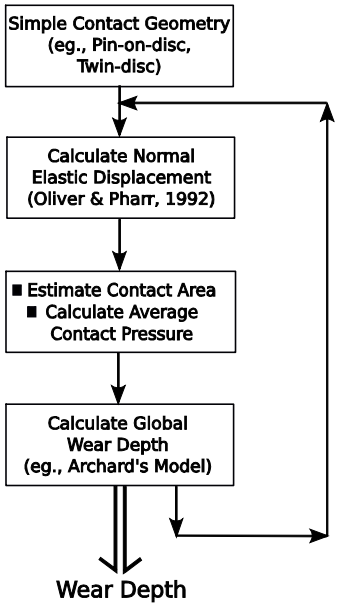

Figure 3: Flow chart of the Global Incremental Wear Model (GIWM)

To predict wear in the micro planetary gear train, the experimentally observed wear behaviour needs to be represented by a wear model, which is able to describe the relevant wear phenomena. One of the most popular wear models as discussed in the introduction is Archard's model [8], which is based on the assumption that the contact pressure p and the sliding distance s between the two contacting surfaces are the major influencing factors for the wear depth h and is written in the form:

$$\frac{dh}{ds} = k_D p \,. \tag{1}$$

The material properties as well as the other influencing parameters, such as environmental conditions, are included in the wear coefficient k_D and have to be identified from experiments. The correct determination of k_D from experimental data is however difficult, because contact pressure and in case of the twin disc tribometer also the slip rate ds/dt are continuously changing during the course of the experiment. In pin-on-disc and twin-disc experiments, wear changes the geometry of the contacting bodies causing a flattening of the pressure profile in the contact [6].

The iterative optimization procedure for parameter identification using full numerical simulations is computationally very intensive [16]. Therefore a Global Incremental Wear Model (GIWM) which is a computationally efficient incremental implementation of Archard's wear model on the global scale for modeling sliding and rolling/sliding wear

has been developed specifically for the pin-on-disc and twin-disc setup. The flow chart for the GIWM is shown in Figure 3. In case of tribo-systems with simple geometries, especially for tribometers (e.g., pin-on-disc, twin-disc), the estimation of the contact area can be simple. In such cases, it may not be necessary to solve the contact problem using finite elements and instead wear can be modeled on the global scale. The estimation of the contact area in the GIWM is accomplished by considering both the normal elastic displacement and wear which is normal to the contacting surface. From the applied normal load and the estimated contact area, an average contact pressure across the contacting surface is calculated. The average contact pressure (global quantity) is then used in a suitable wear model to calculate the increment of wear depth for a pre-

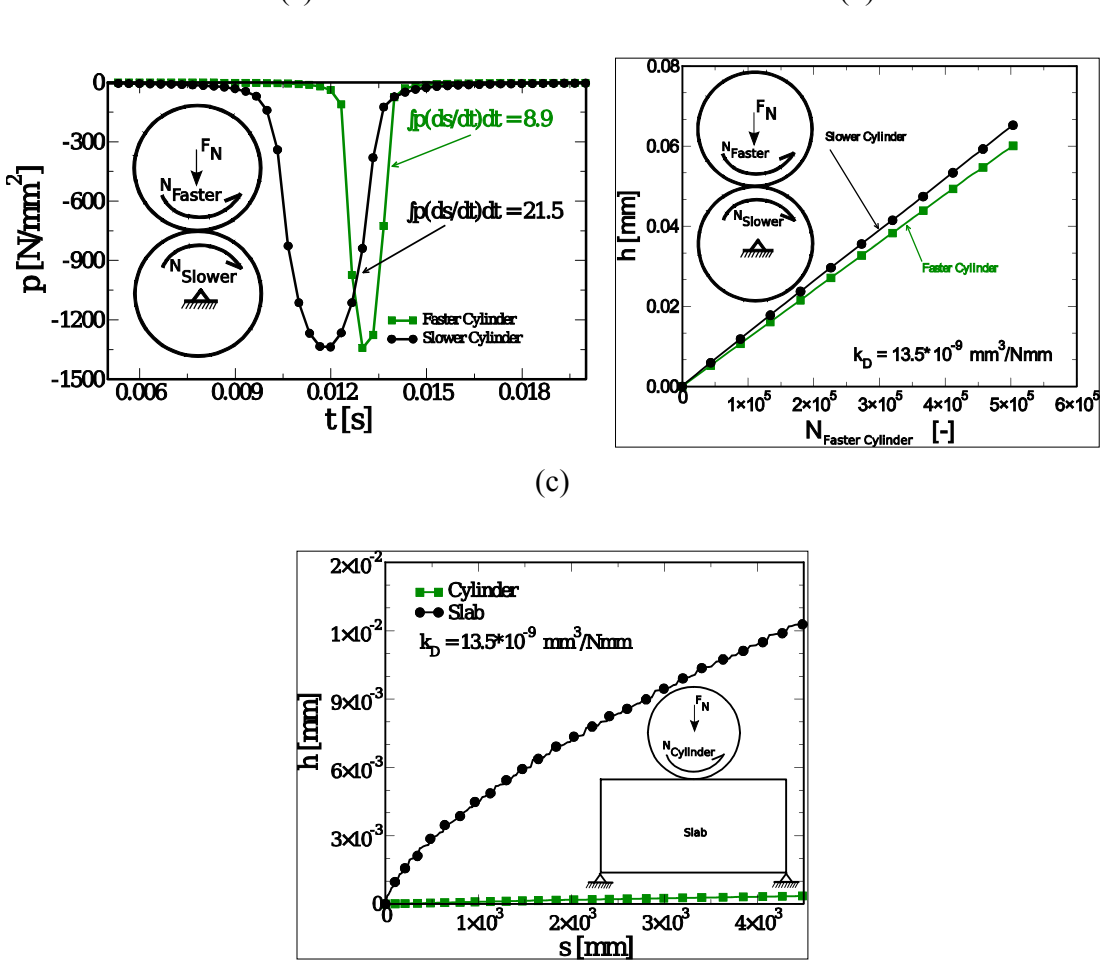

Figure 4: (a) Contact pressure as a function of time in a cylinder on cylinder rolling/sliding contact and (b) the resulting wear as a function of the number of rotation of the lower cylinder which rotates at a comparatively higher speed. (c) Wear depth as a function of the sliding distance as seen by the slab surface.

determined sliding distance increment. The wear depth is then integrated over the sliding distance to get the traditional wear depth over sliding distance curves (see [7] for a detailed description of GIWM along with the algorithm for various tribometer

geometries). The verification of the applicability of the GIWM for wear prediction under unidirectional sliding and sliding/rolling conditions was presented in [7].

For the sake of clarity and completeness of the present article, the results are shown in Figure 2 (b) for the pin-on-disc and Figure 2 (c) and (d) for twin-disc experiment. In the pin-on-disc setup, a loaded spherical tipped pin is in contact with a rotating disc (Figure 2 (a)) and the wear on the pin and the disc is measured. The GIWM was used to fit the wear depth (h) on the pin from the 200 mN normal load experiment (Figure 2 (b)), where k_D was identified to be 13.5×10^{-9} mm^3/Nmm. Later, the identified wear coefficient was used to predict the 400 mN experiment. It can be seen from the graph of the fit for 200 mN and prediction for 400 mN in Figure 2 (b) that the results from the GIWM are in good agreement with the experiments. A sketch of the twin-disc setup is presented in Figure 2 (a), where the upper and lower discs have a curved and a flat flank, respectively. The loaded and rotating upper disc is in contact with the lower disc rotating at a different speed in the same direction and the wear on the disc surfaces are measured. The GIWM was used to fit the wear volume (V_w) satisfactorily for 4 % slip considering the experimental uncertainty as shown in Figure 2 (c). The wear coefficient, k_D was identified to be 3.3×10^{-8} mm^3/Nmm and 1.5×10^{-8} mm^3/Nmm from the fit for the two discs respectively. The identified wear coefficient was then used to predict the wear volume for a higher slip. Figure 2 (d) shows that the GIWM can predict the wear volume with reasonable accuracy for both the discs at 10 % slip. The data presented in Figure 2 (b) – (d) are for silicon nitride with Young's modulus of 304 GPa and Poisson's ratio of 0.24. The reason for choosing different wear coefficients for the two discs in the twin disc setup is due to the fact that the ceramic disc samples came from different sources and had very different microstructure and surface characteristics.

The above results show that Archard's wear model is applicable for sliding and sliding/rolling contacts within the planetary gear train that we consider in this work. Even for identical samples in the twin-disc setup, the slower disc will experience higher wear. In order to understand why the slower disc experiences comparatively higher wear, we consider two cylinders in contact with identical diameters and material properties but rotated at different speeds. For the slower cylinder, the integral of the product of the pressure p and slip rate ds/dt with respect to time is higher (Figure 4 (a)) which is the quantity according to the Archard's wear model (see Equation 4) that is multiplied with the wear coefficient, k_D after each cycle to calculate the increment of the wear depth. As a result the slower cylinder experiences higher wear compared to the faster cylinder as shown in Figure 4 (b). In the extreme case when the slower cylinder is made stationary or if we assume a contact between a rotating cylinder and a flat stationary slab, the stationary tribo-element undergoes very high rates of wear as the rotating cylinder begins to dig into the stationary slab as shown in Figure 4 (c).

After identification of k_D and verification of Archard's wear model for sliding and rolling/sliding contact, it is implemented in an advanced transient formulation of the Wear Processor [16] and applied to simulate wear on mating gear tooth which is presented in section 4 of this article. But, before we proceed with the wear simulations, it is important to perform a finite element contact analysis of the complete planetary gear

train for understanding the contact forces that are generated in a running gear train for identifying the critical areas for wear simulation.

3 Contact analysis of the micro planetary gear train

In this section, we present the finite element contact analysis of the complete micro planetary gear train. The finite element model used for this analysis is presented in Figure 5. The planetary gear train is modelled in 2D and the inertia of the moving parts outside the modelled plane is explicitly considered with the inertia added to the in-plane rigid

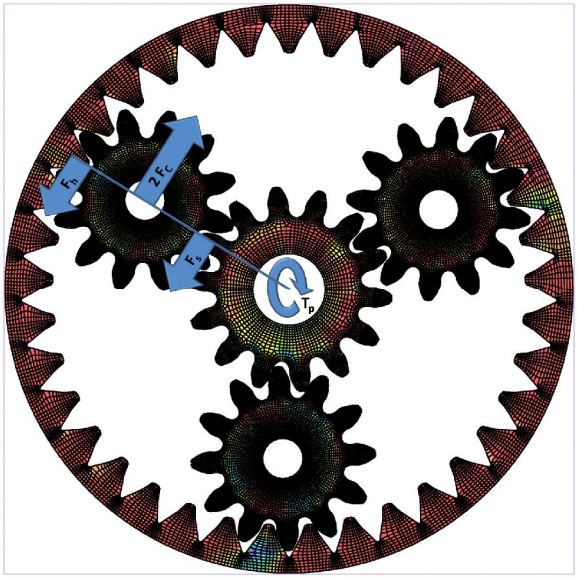

Figure 5: Finite element mesh of the micro planetary gear train (see Figure 1) in 2D.

parts that replace them. The planet gear carrier is replaced by three rigid shafts which are driven by a torque and are forced to stay on their circular path by a pinned reference point at the model's centre. The sun gear's shaft is removed from the model and replaced by explicit rotational inertia so that the motion of the sun gear can be controlled as if it was driven by its shaft. In order to mimic the stiff housing of the gear train in the 2D model, the outer rim of the outer gear is fixed in space. Contact analysis which is nonlinear by nature when applied to such a complex geometry gives a solution that can be mesh density dependent. In Figure 6 (a), the result from the mesh convergence analysis is presented in which the maximum contact force from the simulation at any location and time is used as the parameter to determine the suitability of a particular mesh density. It can be seen from this figure that the mesh with medium density is suitable for our analysis as the results compare favourably with that from the fine mesh and is comparatively less computationally expensive (approximately 90 min on a personal computer with a dual core processor running at 1.83 GHz and a RAM of 1 GB). The medium density mesh has 45988 elements while the fine and coarse density mesh have 95297 and 31447elements respectively.

A simple "back of the envelope" calculation for the gear train in quasi static equilibrium is presented in the following. Assuming that the planetary gear carrier is loaded with a torque T and the sun gear and the outer gear is fixed, there are two forces, one at the contact point between the planet gear and the outer gear (F_h) and the other at the contact point between the sun gear and the planet gear (F_s) which is balanced by a force on the planet gear carrier ($2F_c$). Considering the symmetry of the whole gear train as a first approximation it can be assumed that one of the planet gears is loaded with a torque $T_p = T/3$ acting at the gear train's center. In the ideal case all these forces act in the same tangential direction. Assuming that the center of the planet gear is at a distance R from the gear train's center, in equilibrium we have:

$$\frac{T_p}{R} = F_s + F_h \tag{2}$$

and as the planet gear itself is in equilibrium, $F_s = F_h$. This yields that the force F_c is the same at both positions of contact and can be written as:

$$F_c = F_s = F_h = \frac{T_p / R}{2} = \frac{T}{6R} \tag{3}$$

The force calculated from Equation 3 for different applied torques is presented along with the maximum of the contact force at any location from the finite element analysis in Figure 6 (b). The large difference in the contact force calculated from Equation 3 and finite element analysis is mainly due to the dynamic effects which are implicitly considered in the finite element analysis and also due to the fact that it is the maximum contact force in the finite element model at any instant of time (highest peak in Figure 6 (c) for instance). It is important to note that the results from the FE simulation do not deviate by orders of magnitude from the simple calculation presented above indicating that the boundary conditions used in the calculation are appropriate. We have performed the contact analysis for torques ranging from 5 to 15 Nmm. Fabrication and testing of the prototype is an ongoing work and early tests indicate that the gear train cannot withstand torques of approximately 10 Nmm. Also the "in-service" steady state tangential velocity of the gear train is not known; therefore we have performed analysis at two different tangential velocities differing by an order of magnitude. In Figure 6 (d), the maximum of the minimum principal stress (which gives an idea of the contact pressure in the model) is shown for steady state tangential velocities of 8 and 80 mm/s at the tip of the sun gear. The results show that the increase in the velocity by an order of magnitude has no appreciable effect on the resulting contact pressures. For the analysis, linear elastic material model was used with Young's modulus of 200 GPa, Poisson's ratio of 0.25 and a density of 6 g/cm^3.

It can be concluded from the above analysis of the gear train that the task of simulating wear even with linear elastic material behavior and a simple wear model can be very demanding because of transient effects and the large number of contacts number which are rapidly changing over time. A similar system level contact analysis on a micro lobe pump was carried out by Huber & Aktaa [17], where they concluded that a direct use of

the results from such analysis for wear prediction could include significant uncertainties. Therefore it would be relatively easier if critical regions for wear in the gear train is identified and handled separately. One such critical region is the gear tooth

(a) (b)

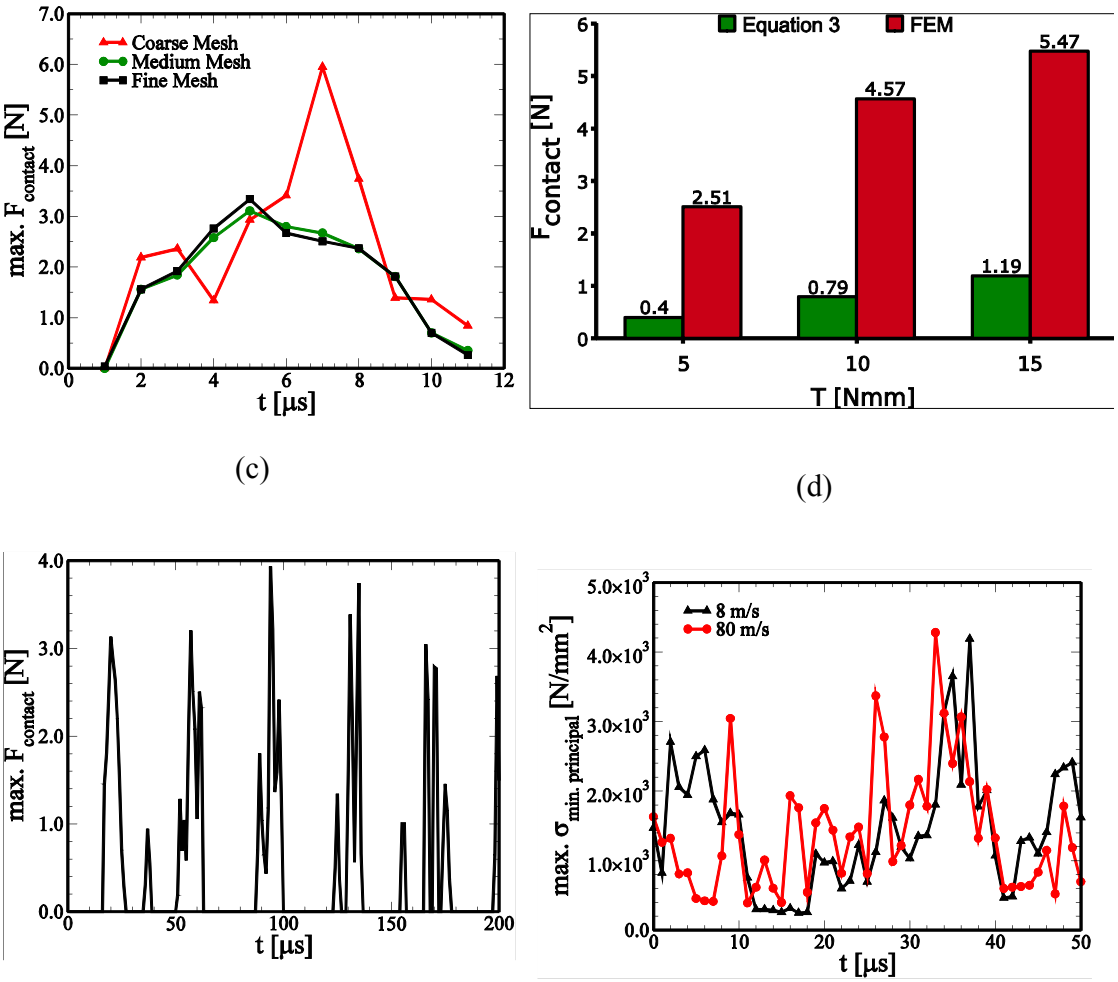

(c) (d)

Figure 6: (a) Maximum contact force as a function of time at any location in the gear train for different mesh densities. (b) Comparison of the force calculated from Equation 3 with the maximum contact force from the finite element simulation. (c) Maximum contact force as a function of time at any location at a higher steady state speed of the gear train compared to that in (a). (d) Maximum of the minimum principal stress as a function of time at any location in the gear train for different steady speeds.

flank which is treated in the next section. Additionally, it would be computationally very demanding to have a good discretisation of the finite element mesh in the complete gear train for satisfactory description of the contact.

4 Wear prediction for rolling/sliding wear on gear teeth flanks

In contrast to pin-on-disc and twin-disc experiments, the contact situation between the

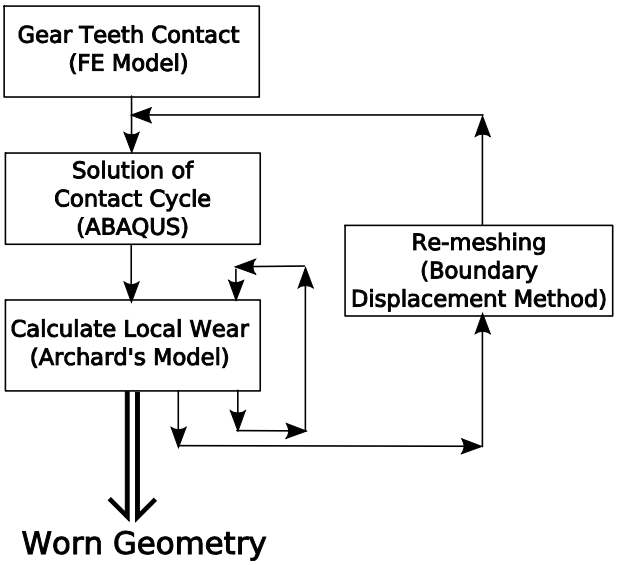

Figure 7: Flow chart of the finite element based wear simulation tool, Wear-Processor

teeth of the planetary gear train is fully transient, i.e. location of contact, pressure and slip rate can rapidly change with time and additionally would change with wear. The simulation of wear under such conditions requires the integration of wear depth using the generalized form of Equation 1

$$dh = k_D p(t) \frac{ds(t)}{dt} dt \,, \tag{4}$$

which has been implemented in the Wear Processor described in detail Hegadekatte et al. [16] and will only be described in brief here for condensing the present article (for similar approaches used by other researchers please see [6] and the literature cited there). The processing of wear begins with the solution of one cycle of rolling/sliding contact between two gear teeth as shown in the flow chart in Figure 7. The solution of this boundary value problem is accomplished with the commercial finite element code ABAQUS. The stress field, the displacement field and the element topology are then extracted from the finite element results file.

The unit inward surface normal vector at each of the surface nodes is computed based on the element topology by averaging the normal vector of the two edge vectors that are connected to each of the surface nodes. The contact pressure for each of the surface nodes on the gear tooth flank is calculated using the extracted stress field and the calculated normal vector. An explicit Euler method is used to integrate Archard's wear law for each surface node over the contact cycle using Equation 4.

The calculated wear from Archard's wear model is used to update the geometry by repositioning the surface nodes with an efficient re-meshing technique that makes use of

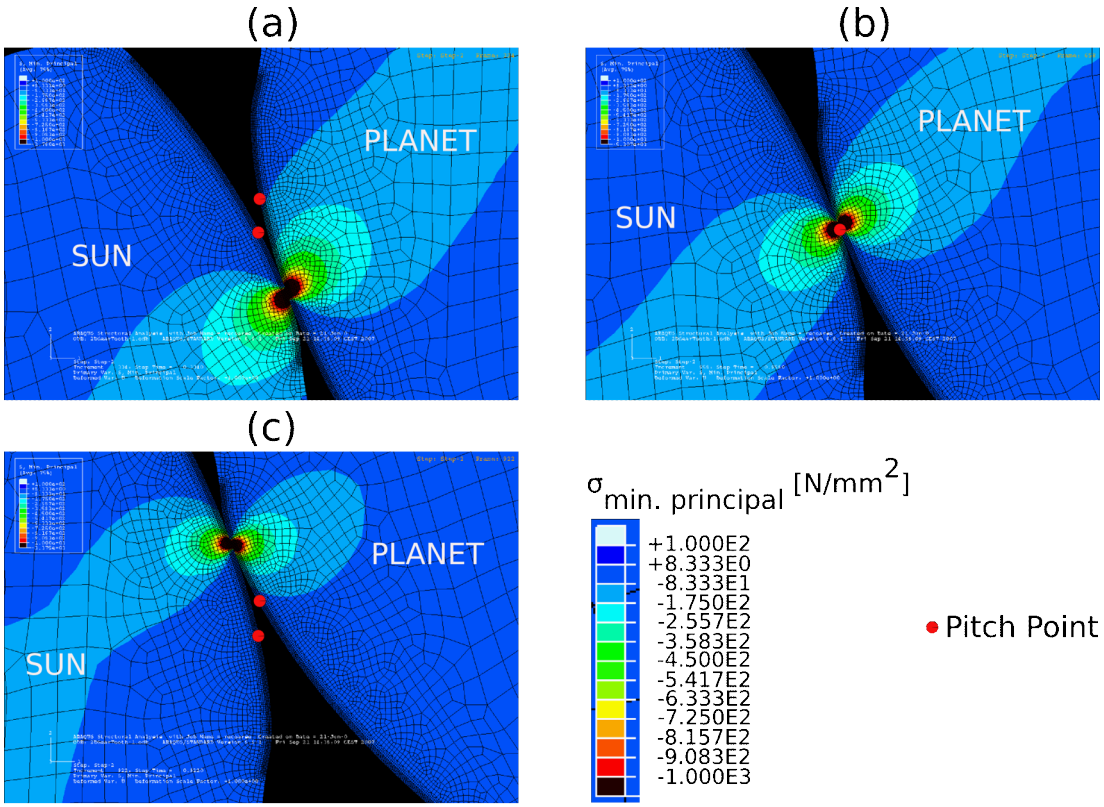

Figure 8: Minimum principal stress field on the flanks of the rotating sun and planet gear teeth at the beginning of contact (a), when the contact reaches nearly the pitch point (b) and the end of the contact cycle (c).

the boundary displacement method (see [16] for more details). The obtained new reference geometry is used to get the updated stress distribution by solving the contact problem again, which in turn is used to compute the updated contact pressure and slip rate distribution. The procedure is continued till a pre defined maximum contact cycle is reached after which the worn geometry can be visualized. As an extension to our previous work, we have implemented an algorithm to map within the contact areas pressure and slip values from the slave surface to the master surface for each time increment. This allows for a simultaneous wear calculation of both contacting gear teeth with a single finite element simulation avoiding time consuming switching of the contact surfaces and re-calculation.

Similar approaches have been used by Andersson and coworkers as discussed in the introduction where instead of a full finite element analysis, an elastic foundation model (Winkler surface model in [19]) or a combination of finite element analysis and an analytical solution of the contact pressure (Hertz [20] solution for elastic non-conformal contacts) has been used to accelerate the simulation [13-15]. It should be noted, that clearly the finite element approach presented here is on one hand time consuming but on the other hand it allows the prediction of geometry change due to wear without any assumptions on the developing tooth profile.

Figure 8 depicts three representative situations for the contact between a tooth of the sun gear and a planetary gear. A torque of 1.5 Nmm is kept constant for the driven planetary gear. While the sun gear tooth turns from left to right, slip decreases, becomes very small at the pitch point and then increases again. At the same time the contact pressure (represented by the minimum principal stress in Figure 8) decreases continuously caused by the increasing lever of the sun tooth. Because the contact area is not limited to a point, there are situations, for which the product of pressure and slip rate are non-zero even at the pitch point and added to it is the fact that the gears are not ideal when they are fabricated as discussed in the introduction. Figure 8 (a), (b) and (c) clearly show that the

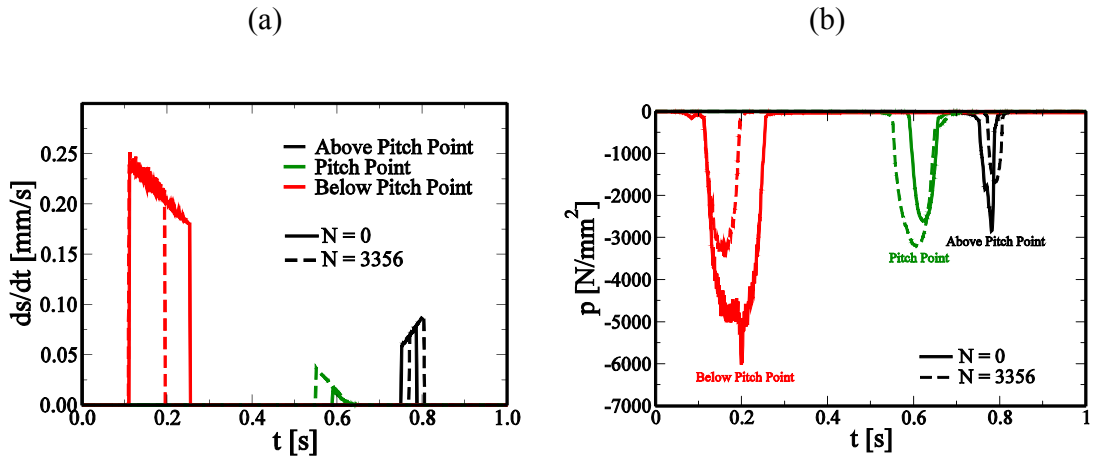

Fig. 9: (a) Variation of slip rate with time and (b) variation of contact pressure and contact area with time at different locations on the flank before and after wear.

slip direction changes during the contact cycle which is due to the fact that the pitch point is nearer to the root of the gear tooth.

The resulting variation of the slip rate *ds/dt* and the contact pressure *p* has been computed before and after wear at 3356 rotations of the sun gear assuming that both gears are made of silicon nitride ($k_D = 3.3 \times 10^{-8}$ mm^3/Nmm). It can be seen from the results shown in Figure 9 (a) and (b), that wear has a significant effect on the evolving contact areas and pressures while the slip rate seems to be independent and simply a function of the current contact location.

There is a considerable change in the contact area and pressure in particular below the pitch point, which results from the larger product of slip and pressure in this region. Surprisingly, the geometry changing wear tends to equalize contact pressure and area for

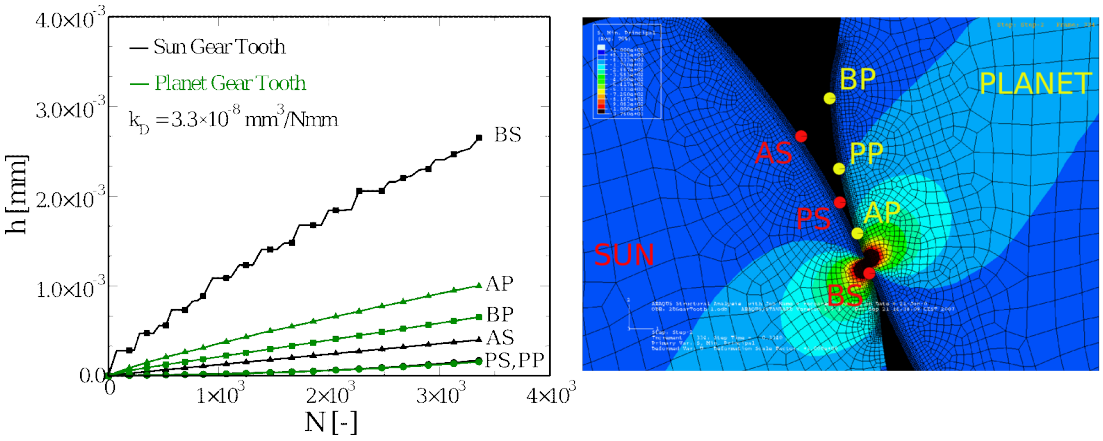

Figure 10: Wear depth over number of rotations of the sun gear at different locations on the sun and the planet gear tooth.

the three locations independent of the increasing lever with time. Although the contact in the pitch point has in theory for ideal gears will have zero slip rate (which should result in zero wear according to Equation 4), it can be seen that the contact variables are still changing. The reason for this phenomenon is the extension of the contact area, which leads to a positive pressure in the pitch point shortly before and after the zero slip condition. The resulting wear depths are presented in Figure 10. The highest amount of wear depth is about 3 µm and is reached below the pitch point while the lowest values are observed in the pitch point, as it can be expected from the previous discussion. Similar conclusions were given by Wu & Cheng [12] while experimentally verifying their wear model. For a gear tooth with a typical dimension of 200 µm in width along the pitch circle, this amount of wear after about 3500 revolutions can be considered as being

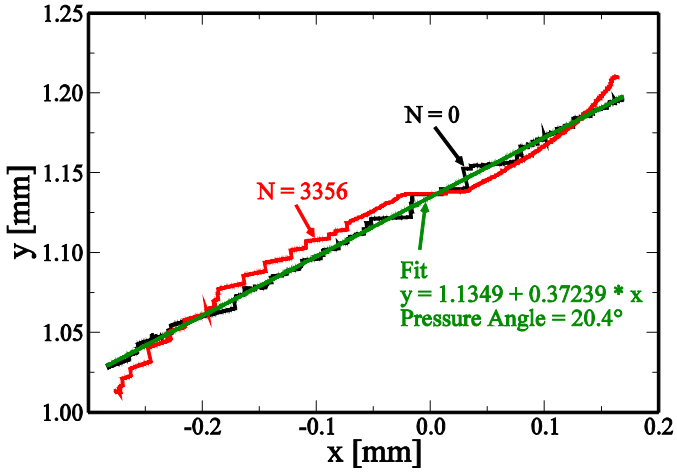

Figure 11: Graph showing the change in the trajectory of the line of action with wear.

significant.

Figure 11 shows a visible change in the kinematics of the gears by plotting the line of action before and after wear. The green line represents the initial line of action given by the initial pressure angle of the gear, which is in excellent agreement with the contact co-ordinates from the simulation before wear (black line, N=0). After wear (N=3356), the "line of action" plotted in red has reached a nonlinear shape, which clearly deviates from the ideal slope.

4 Conclusion and outlook

In this paper, a complete chain has been presented consisting of tribo experiments, the wear model identification and its verification using the GIWM, and finally the transient wear simulation on representative gear tooth flank of a planetary gear train using the Wear Processor.

It can be concluded that the GIWM is a very efficient tool, that allows to determine the wear coefficient(s) of a given wear model. Further, it is very useful to identify the dominant phenomena, especially when it cannot be described by an assumed wear model. This tool allows for identifying the limitations of a wear model and can potentially be used for wear model extension. The deviation between experiments and prediction can be used as a quantitative basis for a further development of wear models like the extension using GIWM that was presented by Steiner el al. [21] for wear in tribological coatings.

The implementation of a fully transient integration scheme in the Wear Processor allows for very general wear simulations on mechanical components. The technique presented in this work is equally applicable in the macro world. The difference in the wear simulation for applications in micro and macro world is the relevant tribo-experiment from where the wear model is identified. The wear depth at a given point does automatically increase for time increments, where the product of contact slip rate and pressure is non-zero. This requires very time consuming simulations using very fine finite element meshes and time stepping. The outcome of this work is however very promising; large numbers of cycles have already been calculated resulting in significant amount of wear with consequences for the gear kinematics. This work represents a significant step forward towards the goal of predicting the effective lifespan and thus enabling more robust design of such complex micro machines.

From our current analysis, it can be expected that the wear has a significant effect on the long-time behaviour of the micro-machine.The goal of our further work is to bridge the time scales as presented here along with the bridging of the length scales. In the present work the boundary condition for the gear tooth simulations did not change with wear but in reality it would change and it needs to be calculated from the complete gear train simulation including statistical analysis of contact conditions which would need bridging different length scales in such highly dynamic systems. Because the time dependent

computation of the contact pressure field from fine meshed models generates an enormous amount of data, the key for reaching this goal will be the development of an efficient integration algorithm for wear in complex systems, where the simulation of time dependent contact forces are sufficient in order to integrate wear over the lifetime of the component.

Acknowledgement

The authors would like to thank the German Research Foundation (DFG) for funding this work under sub project D4 within the scope of the collaborative research center, SFB 499 – Design, production and quality assurance of molded microparts constructed from metals and ceramics. The authors would like to gratefully acknowledge Prof. K. –H. Zum Gahr and Prof A. Albers and their co-workers for the data from tribometry and the prototype of the gear train.

References

[1] Tichy, J. A. & Meyer, D. M. (2000). Review of solid mechanics in tribology. International Journal of Solids and Structures, 37, 391-400.
[2] Gabriel, K., Behi, F., Mahadevan, R., & Mehregany, M. (1990). In situ friction and wear measurements in integrated polysilicon mechanisms. Sensors and Actuators, A21-A23, 184_188.
[3] Williams, J. A. (2001). Friction and wear of rotating pivots in mems and other small scale devices. Wear, 251, 965-972.
[4] Hall, A. C., Dugger, M. T., Prasad, S. V., Christensen, T. (2005). Sidewall Morphology of Electroformed LIGA Parts—Implications for Friction, Adhesion, and Wear Control. Journal of Microelectromechanical Systems, 14, 326-334.
[5] Loehe, D. & Hausselt, J. H. (2005). Micro-Engineering of Metals and Ceramics Part I and Part II. Wiley-VCH Verlag GmbH, Weinheim, Germany.
[6] Hegadekatte, V., Huber, N., & Kraft, O. (2006). Finite element based simulation of dry sliding wear. Tribology Letters, 24, 51-60.
[7] Hegadekatte, V., Kurzenhaeuser, S., Huber, N., & Kraft, O. (2008). A predictive modeling scheme for wear in tribometers. Tribology International, 41, 1020 - 1031.
[8] Archard, J. F. (1953). Contact and rubbing of flat surfaces. J. Appl. Phys., 24, 981-988.
[9] Zhao, Y. & Chang, L. (2002). A micro-contact and wear model for chemical-mechanical polishing of silicon wafers. Wear, 252, 220-226.
[10] Sawyer, W. G. (2004). Surface shape and contact pressure evolution in two component surfaces: Application to copper chemical mechanical polishing. Tribol. Lett., 17, 139-145.
[11] Wu, S. & Cheng, H, S. (1991). A sliding wear model for partial-EHL contacts. ASME Journal of Tribology, 115, 493-500.
[12] Wu, S. & Cheng, H, S. (1993). Sliding wear calculations in spur gears. ASME Journal of Tribology, 115, 493-500.
[13] Flodin, A. & Andersson, S. (1997). Simulation of mild wear in spur gears. Wear, 207, 16-23.

[14] Flodin, A. & Andersson, S. (2000). Simulation of mild wear in helical gears. Wear, 241, 123-128.
[15] Brauer, J. & Andersson, S. (2003). Simulation of gears with flank interference – a mixed FE and analytical approach. Wear, 254, 1216-1232.
[16] Hegadekatte, V., Huber, N., & Kraft, O. (2005). Finite element based simulation of dry sliding wear. Modelling Simul. Mater. Sci. Eng., 13, 57-75.
[17] Huber, N., & Aktaa, J.(2003). Dynamic finite element analysis of a micro lobe pump. Microsystem Technology, 9, 465-469.
[18] Kurzenhäuser, S., Hegadekatte, V., Schneider, J., Huber, N., Kraft, O., Zum Gahr, K.-H. (2008).Tribological characterization and numerical wear simulation of microcomponents under sliding and rolling conditions. Microsystem Technology, 14 (12), 1839 - 1846
[19] Johnson, K. L. (1985). Contact Mechanics. Cambridge University Press, Cambridge, UK.
[20] Hertz, H. (1882). Über die Berührung fester elastischer Körper. J. Reine und Angewandte Mathematik, 92, 156-171.
[21] Steiner, L., Bouvier, V., May, U., Hegadekatte, V., Huber, N. Modelling of unlubricated oscillating sliding wear of DLC-coatings considering surface topography, oxidation and graphitisation. submitted for publication

Figure1

Click here to download high resolution image

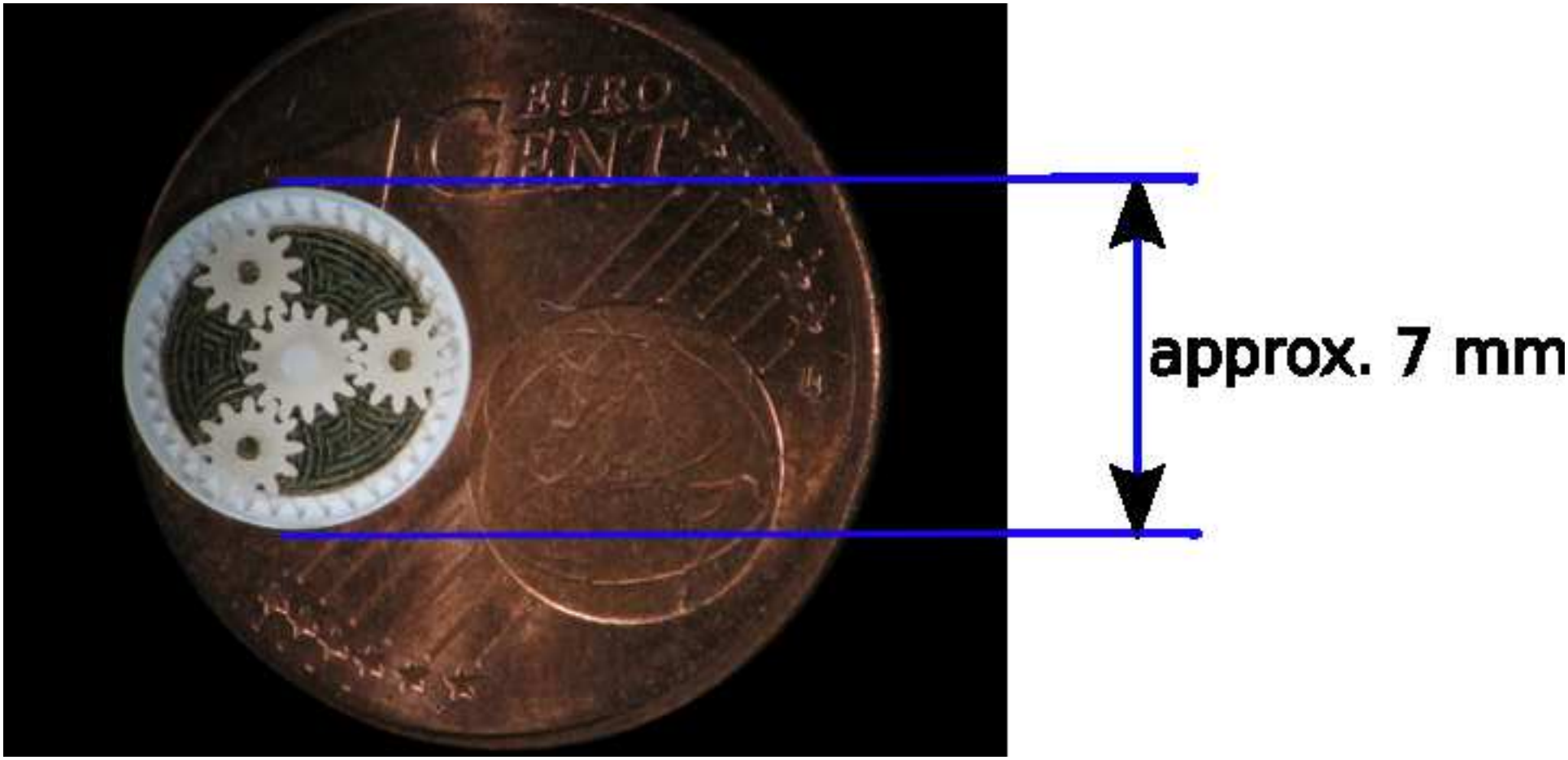

Figure2a-eps

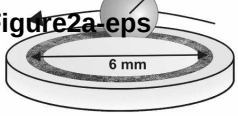

T	= RT
Medium	air, 50% r.h.
	dist. water
pin	ø 1.6 mm
disc	ø 8 x 2 mm²

b)

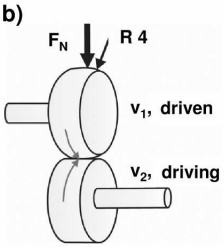

Rolling contact

F_N	= 250 mN
v_1	= 800 mm/s ($v_2 > v_1$)
slip	= 10% (1%, 4%)
N	= 10^6
T	= RT
Medium	air, 50% r.h.
	dist. water
discs	ø 8 x 2 mm²

Figure2a-tif
Click here to download high resolution image

a)

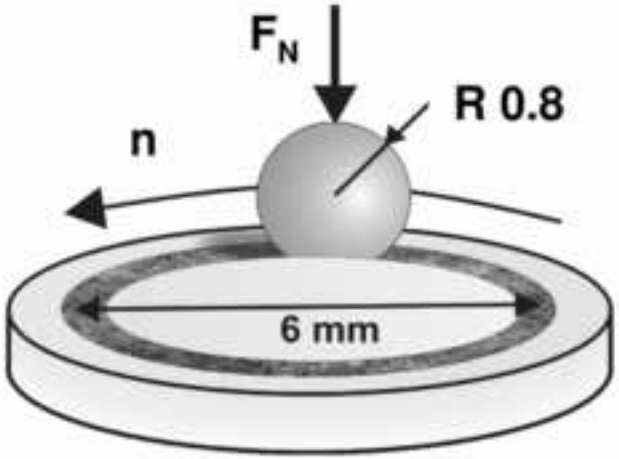

Sliding contact

F_N	= 800 mN
v	= 400 mm/s
s	= 1000 m
T	= RT
Medium	air, 50% r.h.
	dist. water
pin	ø 1.6 mm
disc	ø 8 x 2 mm²

b)

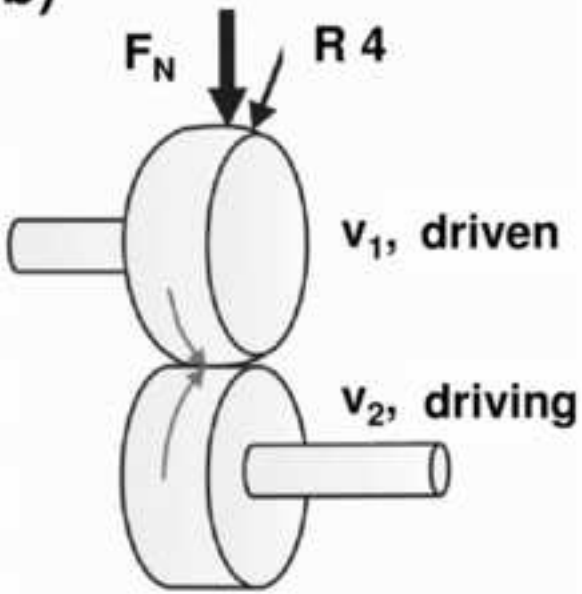

Rolling contact

F_N	= 250 mN
v_1	= 800 mm/s ($v_2 > v_1$)
slip	= 10% (1%, 4%)
N	= 10^6
T	= RT
Medium	air, 50% r.h.
	dist. water
discs	ø 8 x 2 mm²

Figure2b

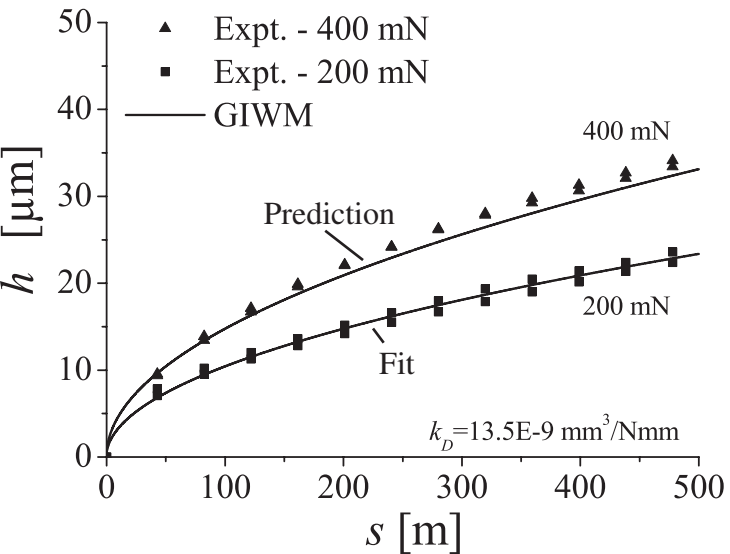
Expt. - 400 mN
Expt. - 200 mN
GIWM
400 mN
Prediction
200 mN
Fit
k_D=13.5E-9 mm^3/Nmm
h [µm]
s [m]
0
10
20
30
40
50
0
100
200
300
400
500

Figure2c

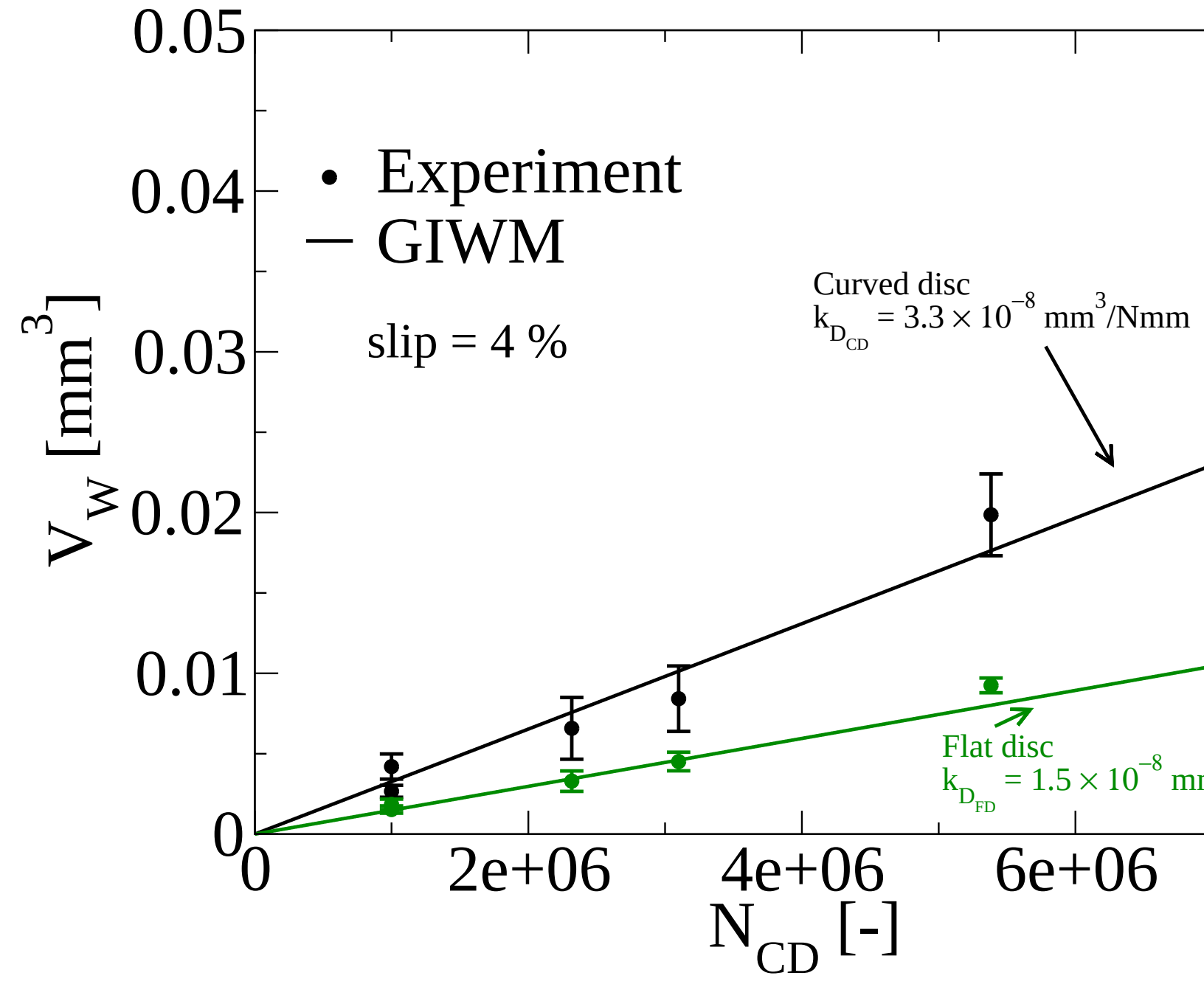
0.05
0.04
0.03
0.02
0.01
0
0
2e+06
4e+06
6e+06
V_w [mm^3]
N_{CD} [-]
• Experiment
— GIWM
slip = 4 %
Curved disc
$k_{D_{CD}} = 3.3 \times 10^{-8}$ mm^3/Nmm
Flat disc
$k_{D_{FD}} = 1.5 \times 10^{-8}$ mm

Figure2d

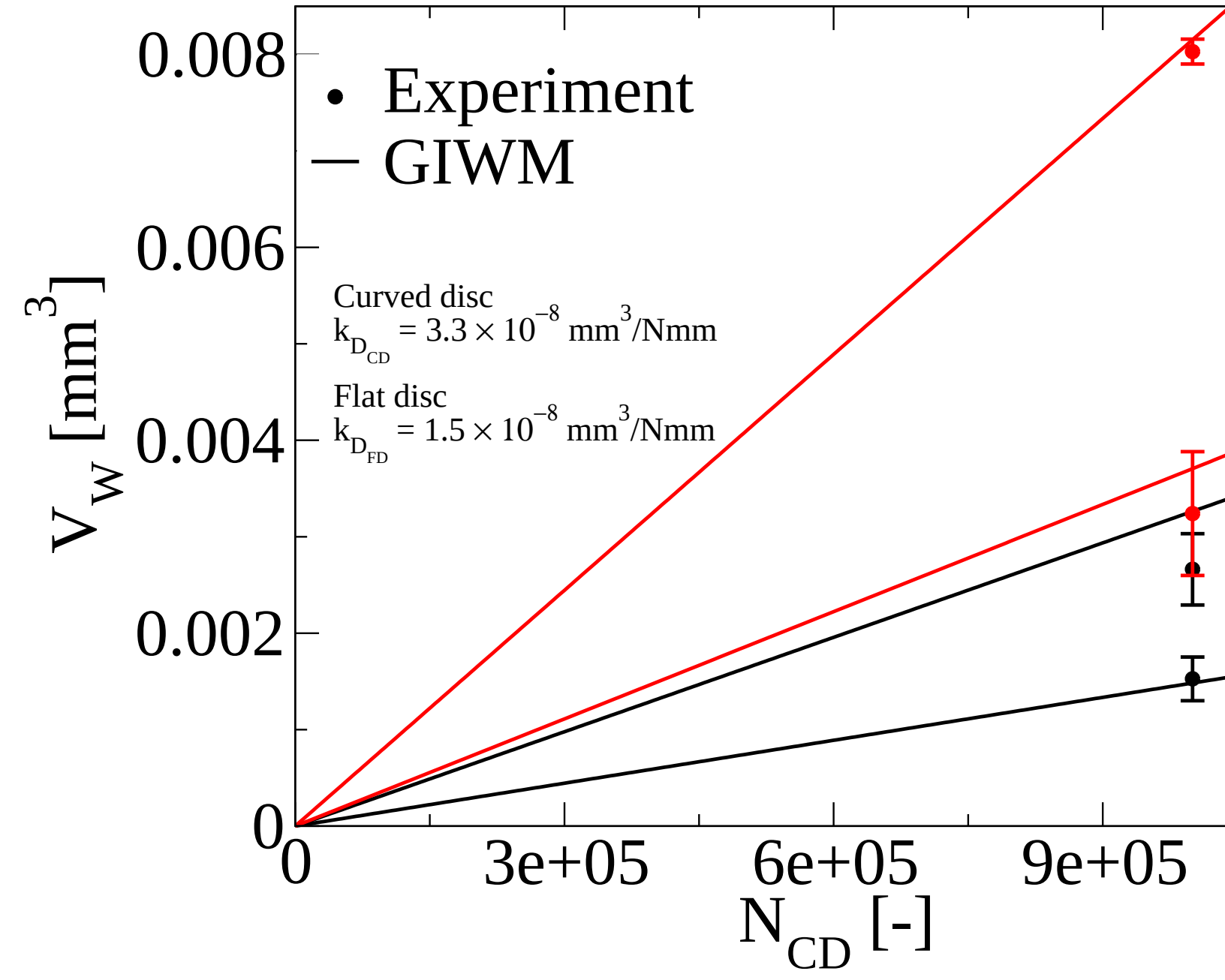
0.008
0.006
0.004
0.002
0
0
3e+05
6e+05
9e+05
V_W [mm^3]
N_{CD} [-]
Experiment
GIWM
Curved disc
$k_{D_{CD}} = 3.3 \times 10^{-8}$ mm^3/Nmm
Flat disc
$k_{D_{FD}} = 1.5 \times 10^{-8}$ mm^3/Nmm

Figure3

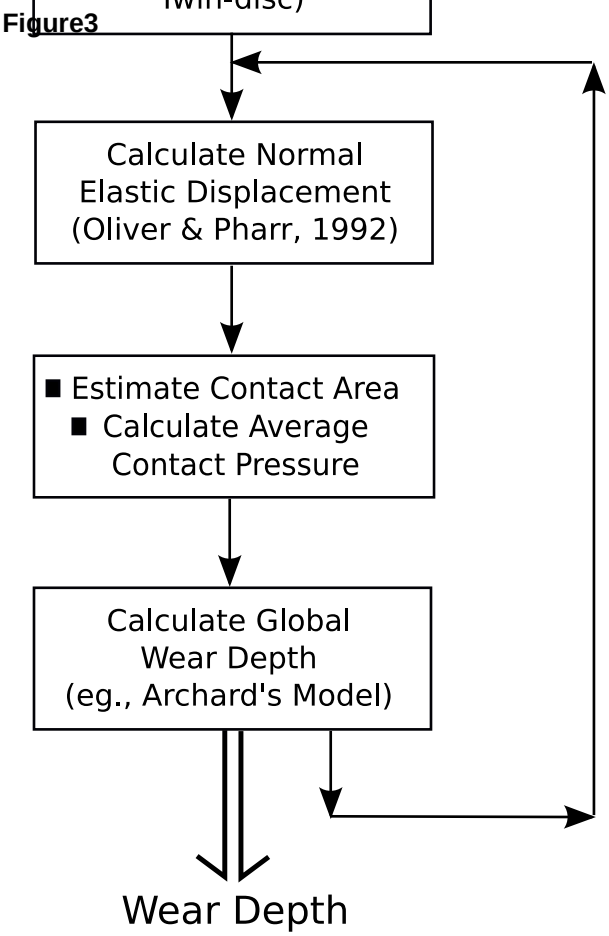
Calculate Normal
Elastic Displacement
(Oliver & Pharr, 1992)
Estimate Contact Area
Calculate Average
Contact Pressure
Calculate Global
Wear Depth
(eg., Archard's Model)
Wear Depth

Figure4a

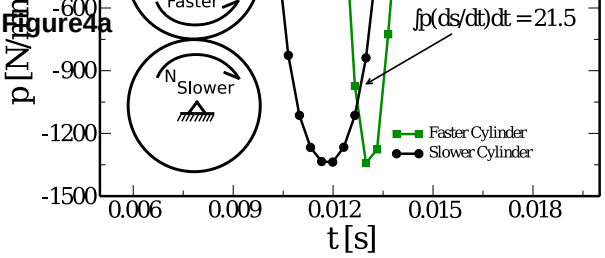
p [N/m]
-600
-900
-1200
-1500
0.006
0.009
0.012
0.015
0.018
t [s]
N Faster
N Slower
∫p(ds/dt)dt = 21.5
Faster Cylinder
Slower Cylinder

Figure4b

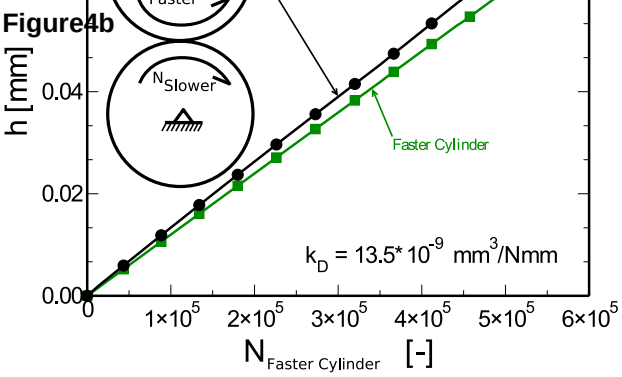
h [mm]
0.04
0.02
0.00
0
1×10^5
2×10^5
3×10^5
4×10^5
5×10^5
6×10^5
N Faster Cylinder [-]
N Slower
Faster Cylinder
k_D = 13.5* 10^-9 mm^3/Nmm

Figure4c

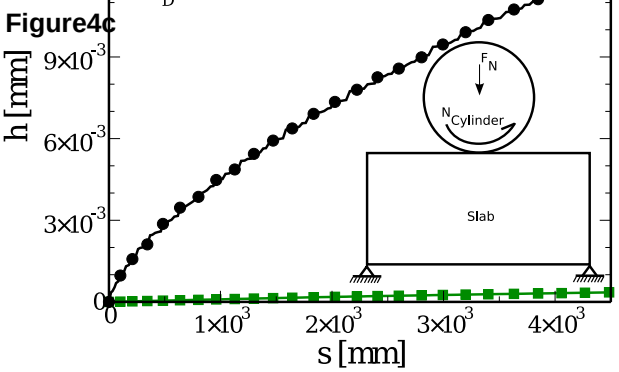
h [mm]
9×10-3
6×10-3
3×10-3
0
0
1×10-3
2×10-3
3×10-3
4×10-3
s [mm]
FN
NCylinder
Slab

Figure5

Click here to download high resolution image

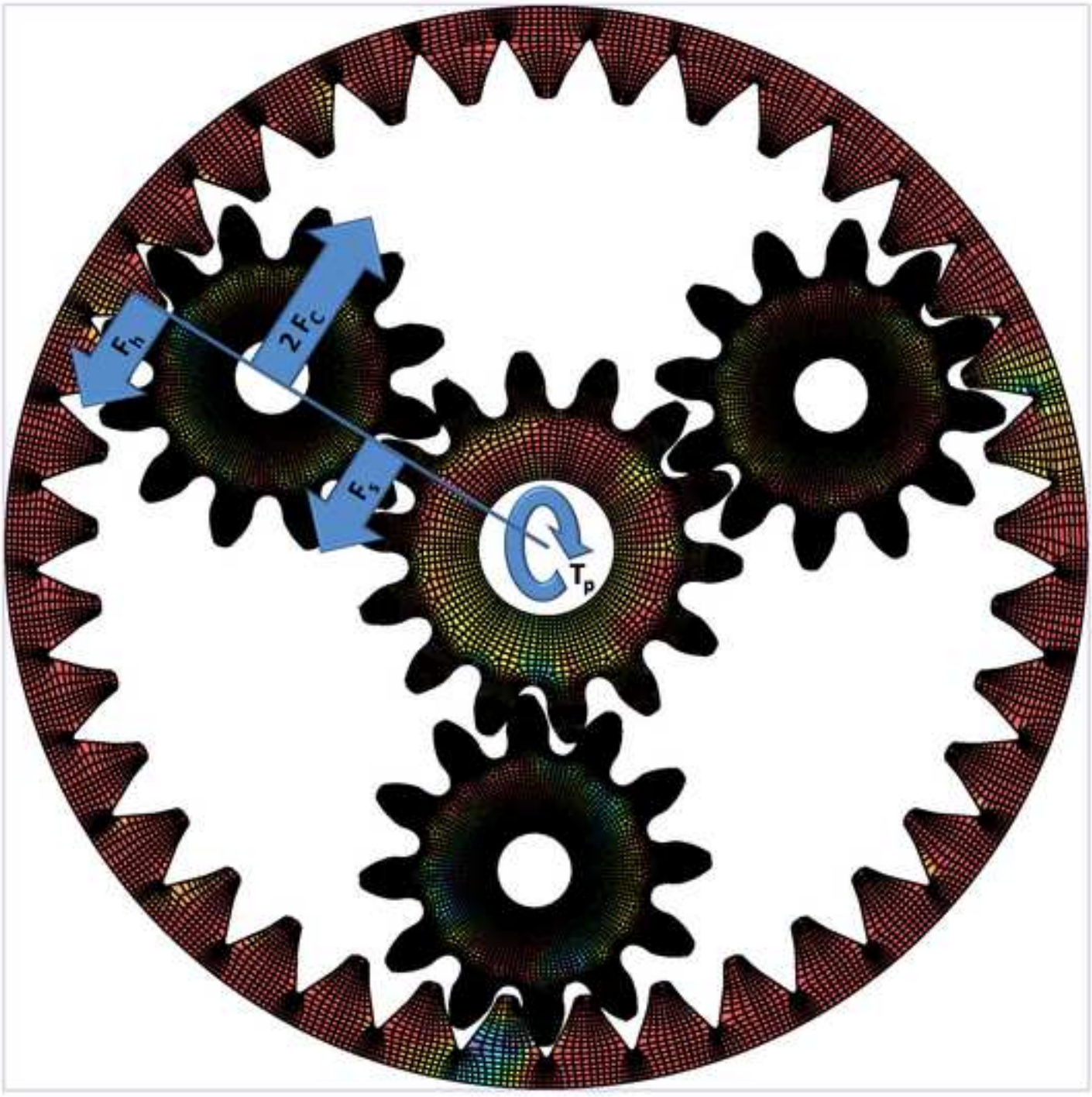

Figure6a

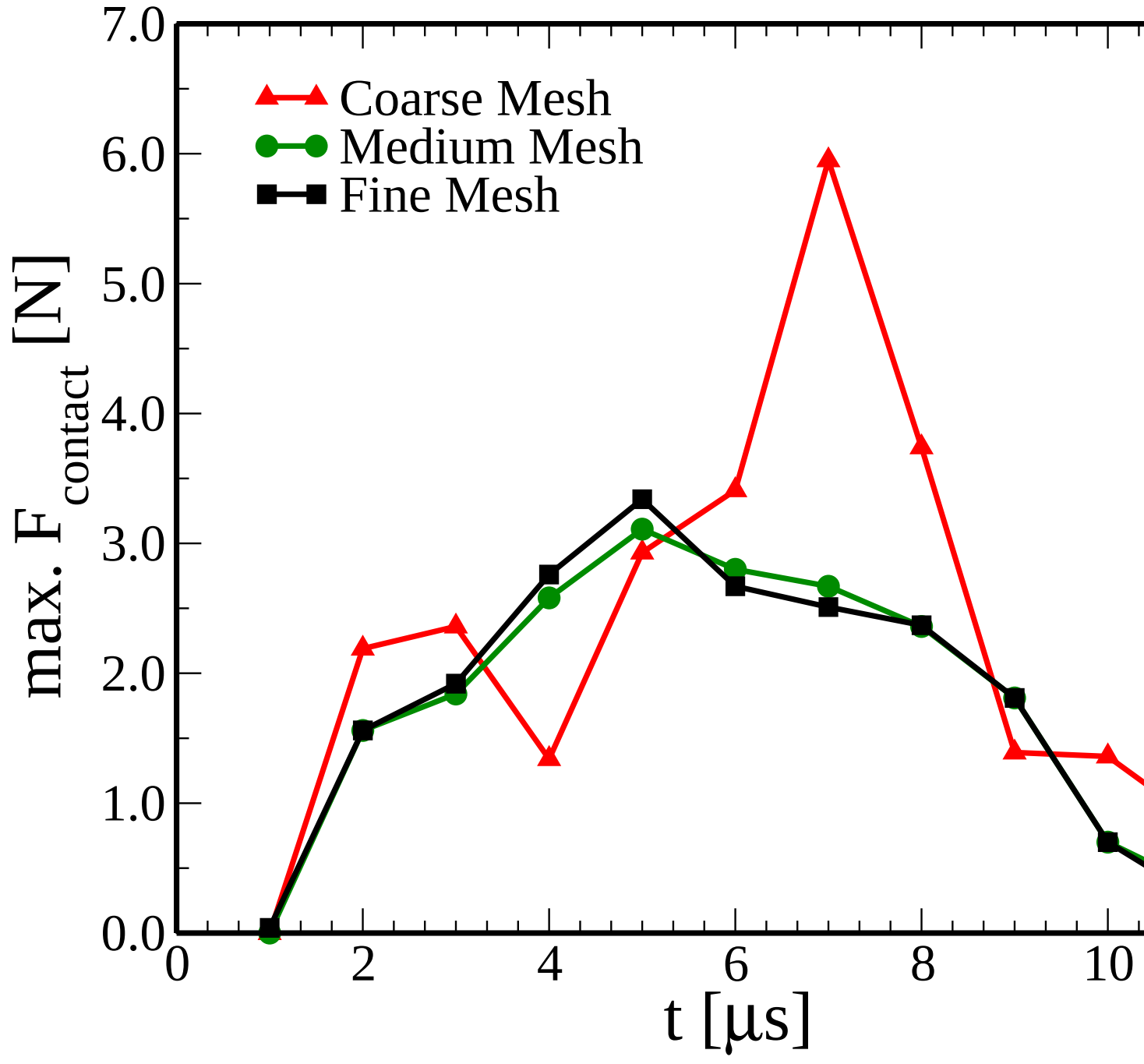
Coarse Mesh
Medium Mesh
Fine Mesh
max. F contact [N]
t [µs]
0.0
1.0
2.0
3.0
4.0
5.0
6.0
7.0
0
2
4
6
8
10

Figure6b

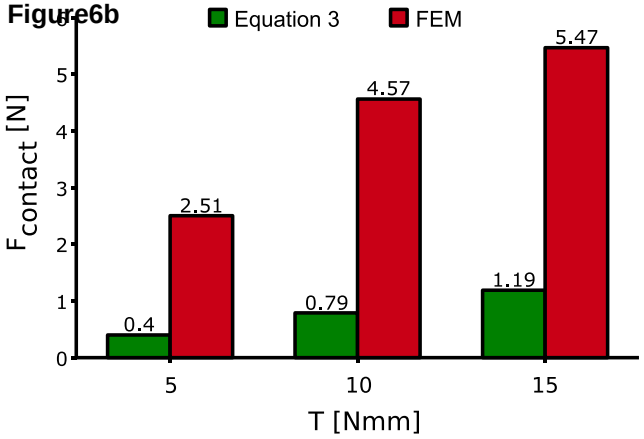
Equation 3
FEM
F contact [N]
0
1
2
3
4
5
6
0.4
2.51
0.79
4.57
1.19
5.47
5
10
15
T [Nmm]

Figure6c

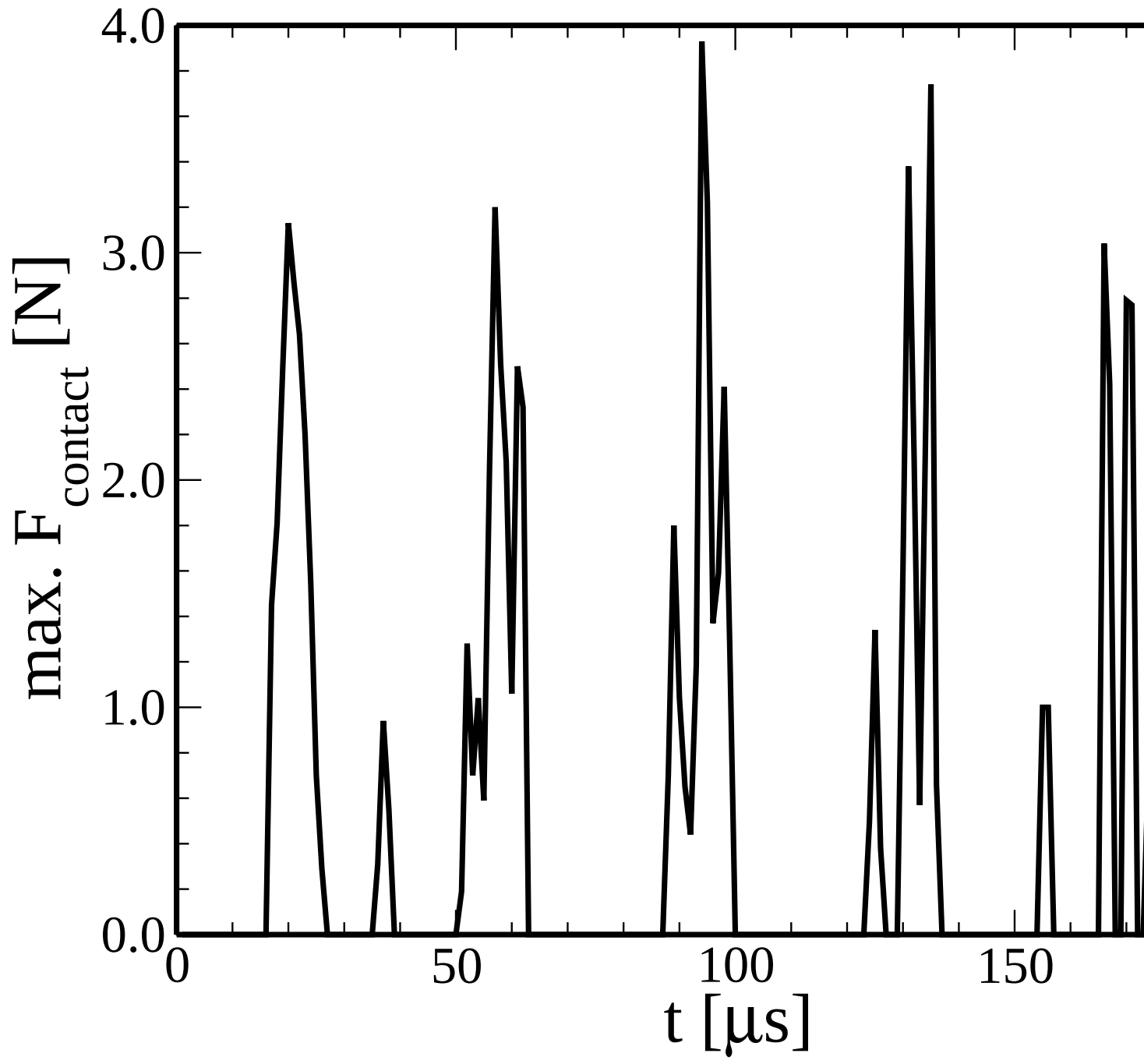

Figure6d

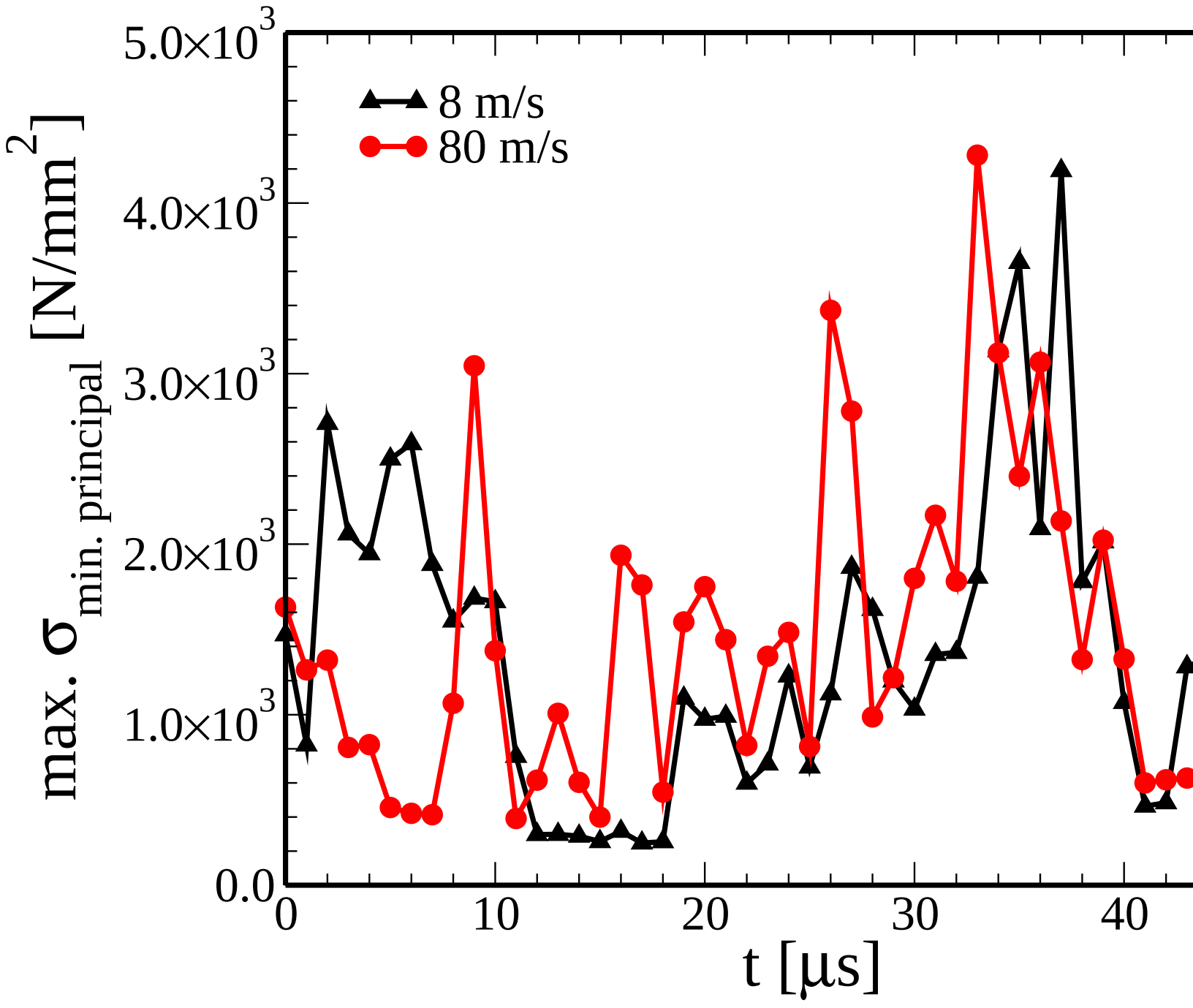
5.0×10^3
4.0×10^3
3.0×10^3
2.0×10^3
1.0×10^3
0.0
0
10
20
30
40
t [μs]
max. σ min. principal [N/mm^2]
8 m/s
80 m/s

Figure7

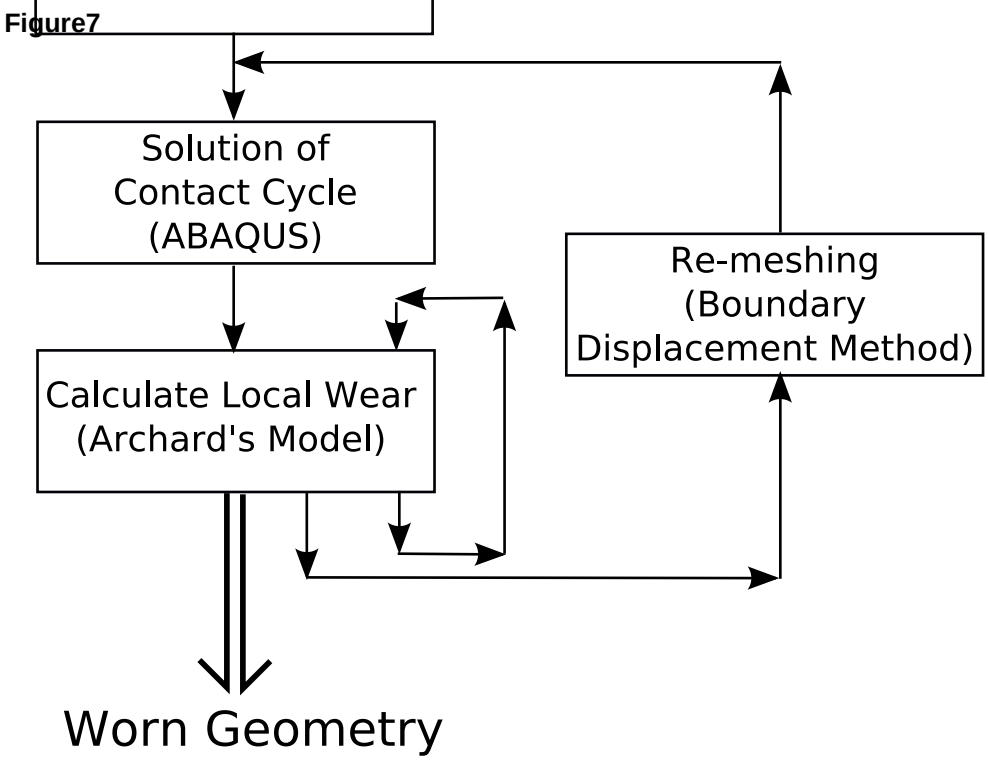
Solution of
Contact Cycle
(ABAQUS)
Re-meshing
(Boundary
Displacement Method)
Calculate Local Wear
(Archard's Model)
Worn Geometry

Figure8abc-eps

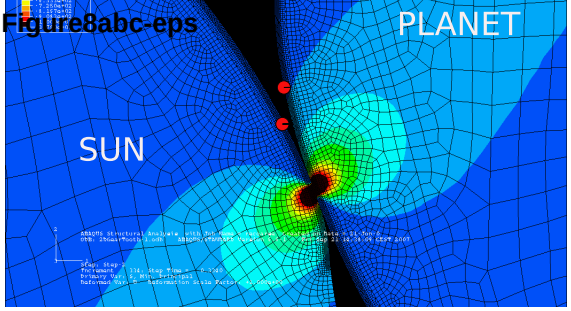

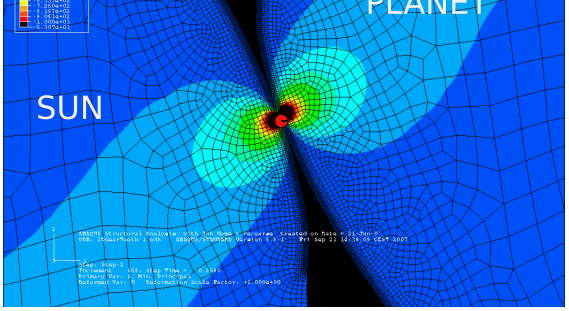

(c)

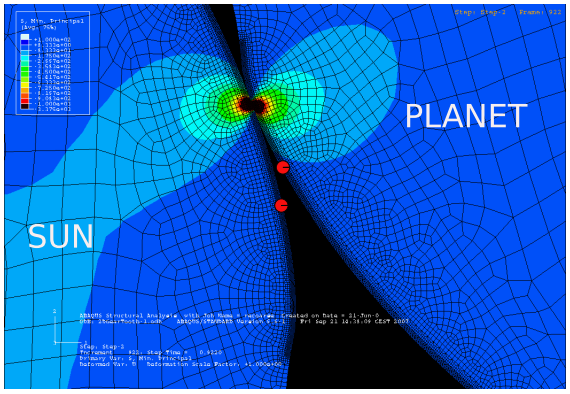

$\sigma_{\text{min. principal}}$ [N/mm^2]

+1.000E2
+8.333E0
-8.333E1
-1.750E2
-2.557E2
-3.583E2
-4.500E2
-5.417E2
-6.333E2
-7.250E2
-8.157E2
-9.083E2
-1.000E3

Pitch Point

Figure8abc-tif
Click here to download high resolution image

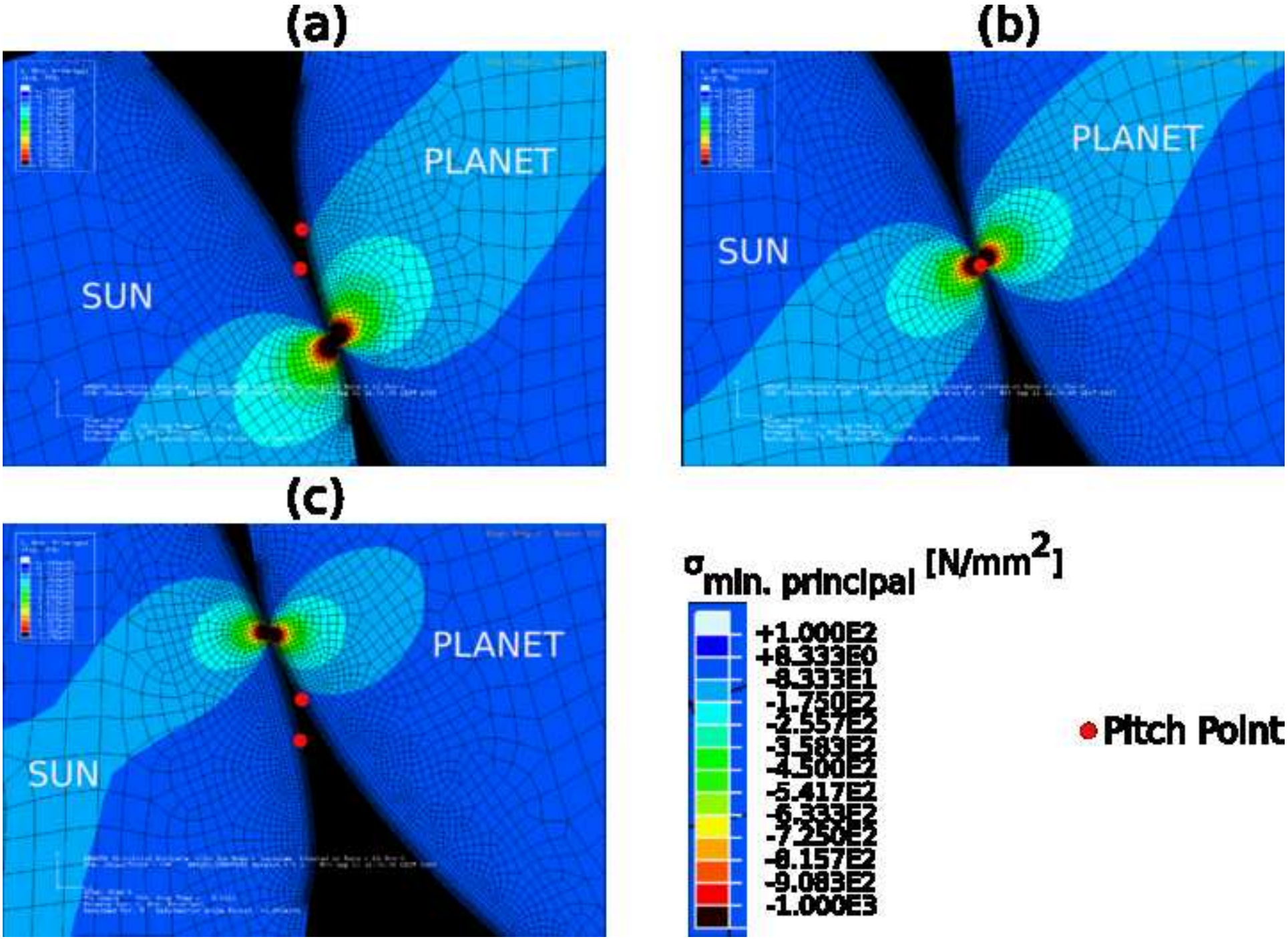

Figure9a

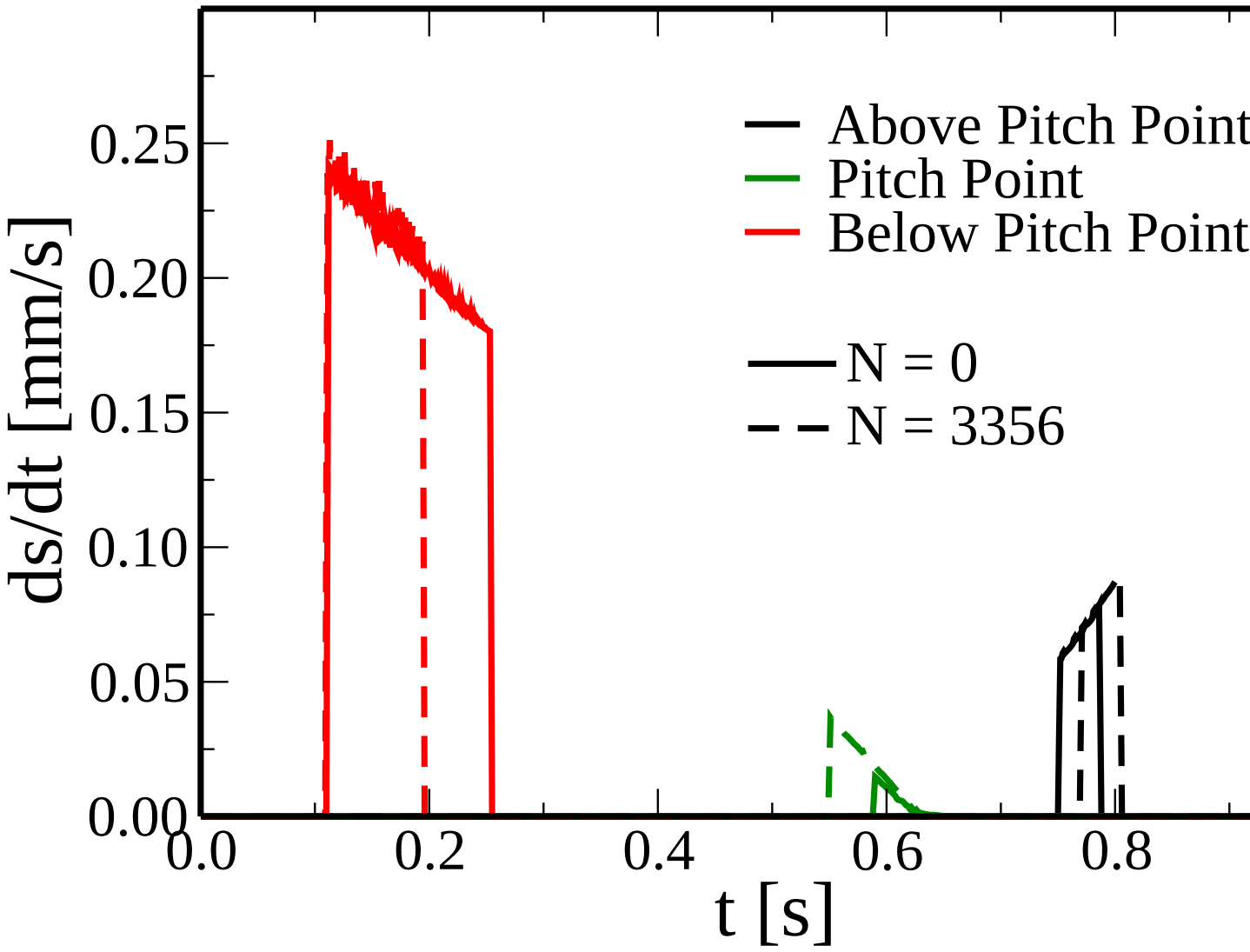
Above Pitch Point
Pitch Point
Below Pitch Point
N = 0
N = 3356
ds/dt [mm/s]
0.25
0.20
0.15
0.10
0.05
0.00
0.0
0.2
0.4
0.6
0.8
t [s]

Figure9b

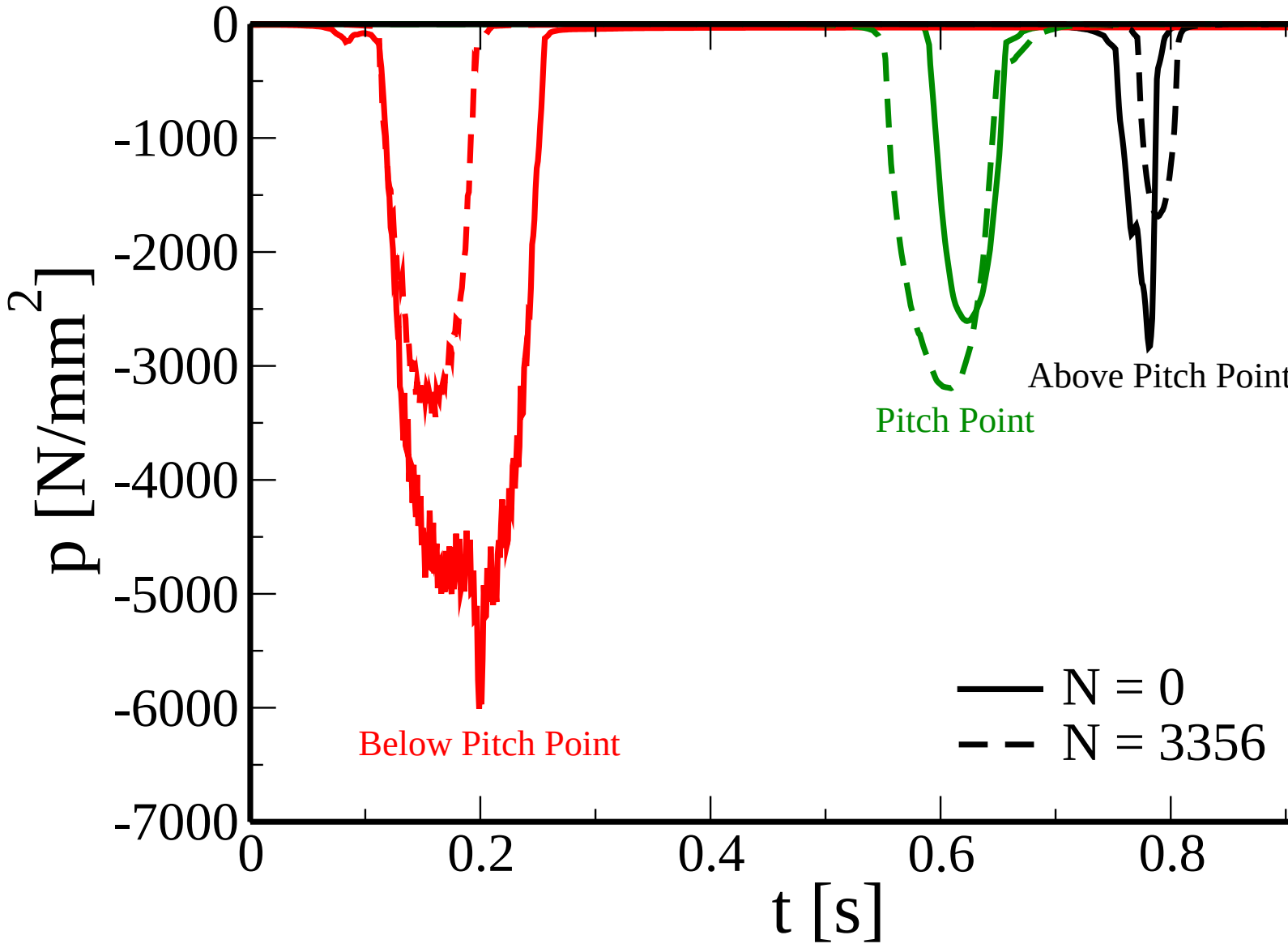
0
-1000
-2000
-3000
-4000
-5000
-6000
-7000
p [N/mm2]
0
0.2
0.4
0.6
0.8
t [s]
Below Pitch Point
Pitch Point
Above Pitch Point
N = 0
N = 3356

Figure10-eps

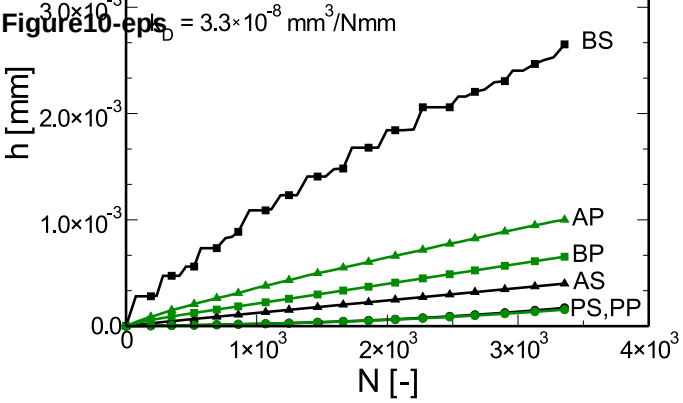

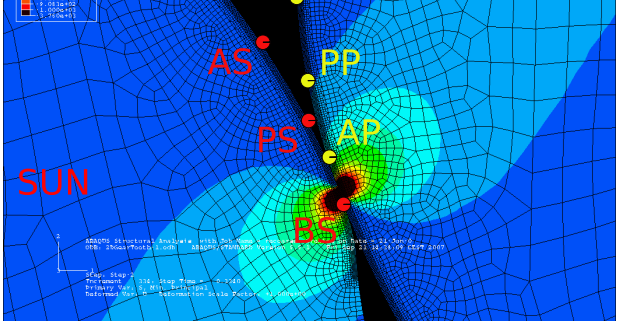

Figure10-tif
Click here to download high resolution image

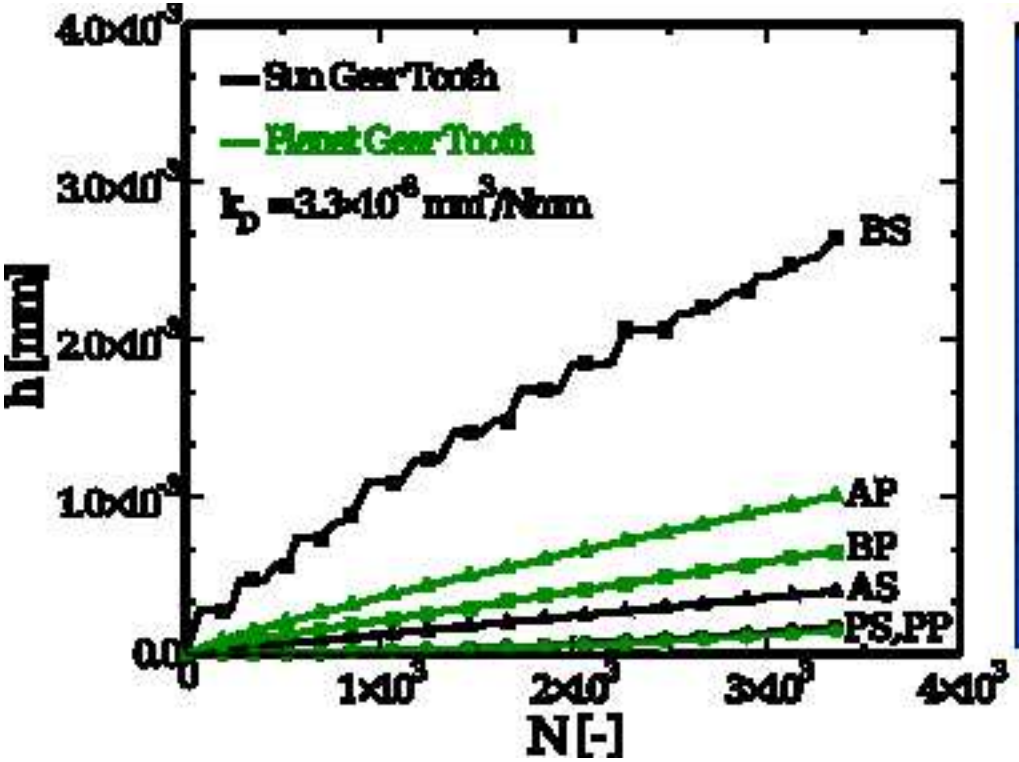

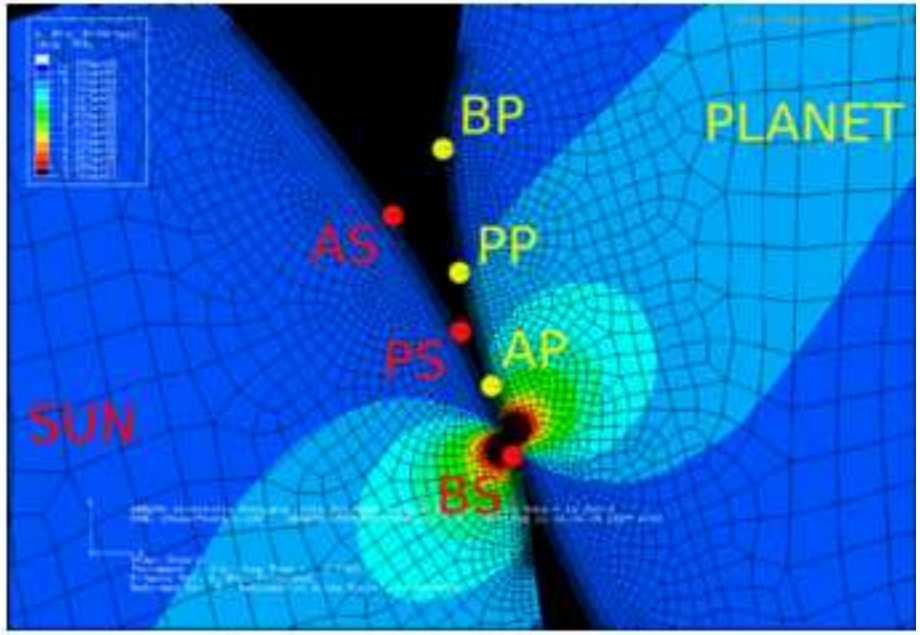

Figure11

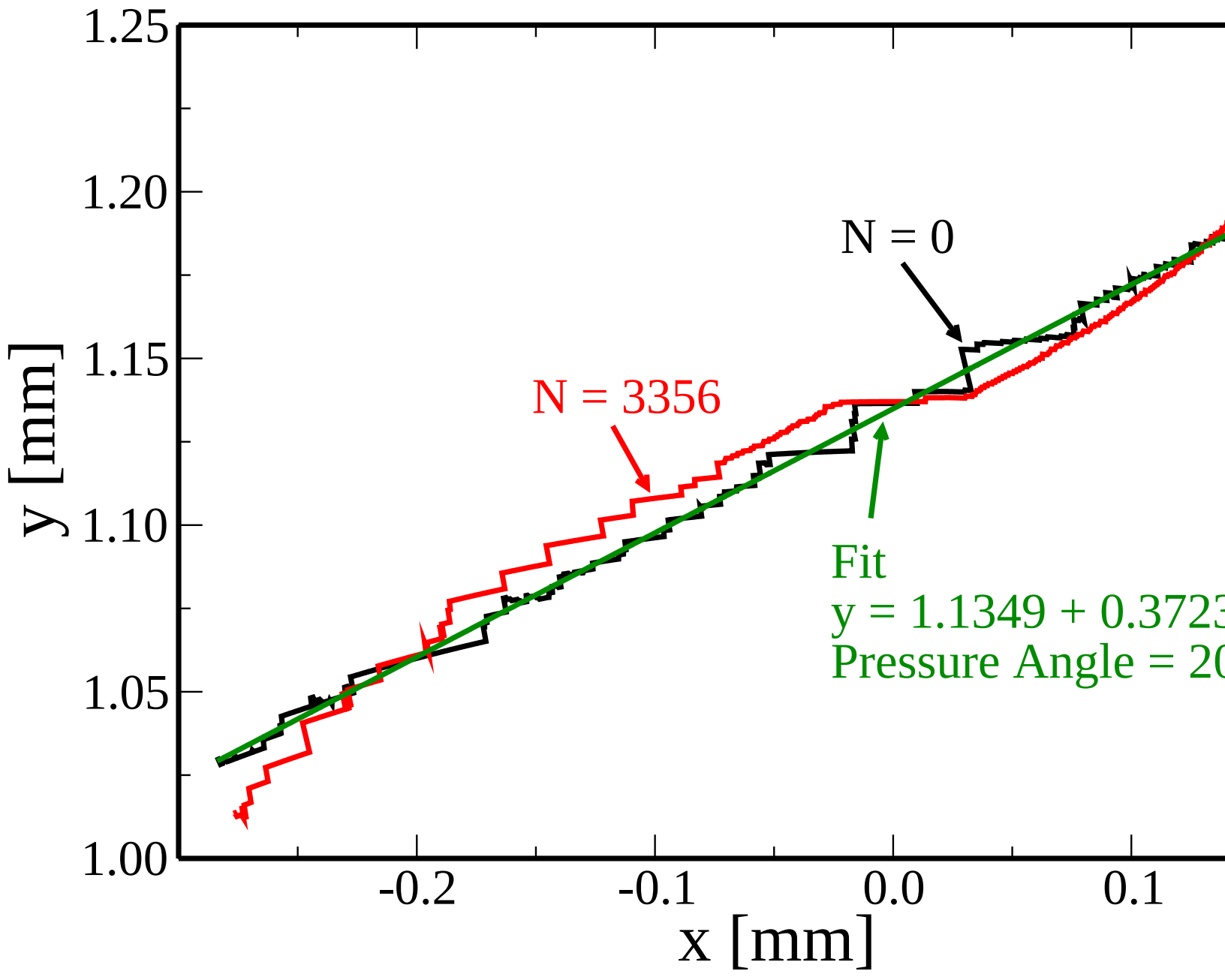
1.25
1.20
1.15
1.10
1.05
1.00
y [mm]
-0.2
-0.1
0.0
0.1
x [mm]
N = 0
N = 3356
Fit
y = 1.1349 + 0.3723
Pressure Angle = 20